Precambrian Research 385 (2023) 106940

Contents lists available at ScienceDirect

Precambrian Research

journal homepage: www.elsevier.com/locate/precamres

Geological processes defining the formation of plumasite-type corundum in the Paleoproterozoic Isertoq Terrane, South-East Greenland

Majken D. Poulsen [a,b,c,*], Nynke Keulen [a], Vincent J. van Hinsberg [d], Jochen Kolb [e], Robert Frei [c], Tonny B. Thomsen [a]

[a] Department of Mapping and Mineral Resources, Geological Survey of Denmark and Greenland (GEUS), Øster Voldgade 10, 1350 Copenhagen K., Denmark
[b] Geological Survey of Denmark and Greenland Nuuk Office, C/o Institute of Natural Resources, Kivioq 2, postboks 570, 3900 Nuuk, Greenland
[c] Department of Geosciences and Natural Resource Management, University of Copenhagen, Øster Voldgade 10, 1350 Copenhagen K., Denmark
[d] GEOTOP Research Centre, Department of Earth & Planetary Sciences, 3450 University Street, Montreal, Quebec H3A 2A7, Canada
[e] Karlsruhe Institute of Technology, Institute of Applied Geosciences, Geochemistry and Economic Geology, Adenauerring 20b, D - 76131 Karlsruhe, Germany

ARTICLE INFO

Keywords:
Ultramafic rocks
Nagssugtoqidian Orogen
Metasomatism
Pegmatite
U-Pb zircon dating

ABSTRACT

Plumasite-type corundum occurrences in the Nattivit area in South-East Greenland offer a unique opportunity to study corundum formation *in-situ* where pegmatites intruded into metamorphosed lherzolite and dunite of the Archean-Paleoproterozoic continental crust. The Nattivit area, located in the Isertoq Terrane of North Atlantic Craton, forms part of the overriding plate during convergence of the Nagssugtoqidian orogen (1910-1840 Ma). New field observations and elemental and isotopic geochemical analysis provide further insights in the history of crustal convergence, its exhumation and how corundum was formed. The continental crust in the area consists of metamorphosed mafic to ultramafic rocks and tonalite-trondhjemite-granodiorite (TTG) gneisses, where the mafic rocks in the Isertoq Terrane yield a εNd T_{DM} model age of 3000–2800 Ma. Dunite and lherzolite sills/dikes intruded the mafic rocks before the intrusion of the TTG sheets. The intrusion ages for the TTG obtained from zircon U-Pb geochronology are 2818 ± 8 Ma, 2760 ± 13 Ma to 2667 ± 7 Ma. U-Pb zircon data, zircon textures and Th/U ratios indicate metamorphism occurred at 2698 ± 7 Ma to 2629 ± 11 Ma, 2500–2400 Ma and 1900–1600 Ma. Whole rock geochemical data of mafic to ultramafic rocks show a continental arc affinity, with negative Ta, Nb and positive Pb anomalies. A metasomatic event at 2390 ± 70 Ma partly reset the isotopic signature in the mafic to ultramafic rocks. A marked absence of ages between 2350 and 2100 Ma in the TTG zircon age populations exists, indicating a period with minimal magmatic and/or metamorphic activity. The metamorphic mineral assemblages of the schist, amphibolite, ultramafic rocks and metasomatic reaction zones in ultramafic rocks indicate upper to medium–high amphibolite facies conditions. Kyanite in the metasomatic reaction zones in ultramafic rocks indicate the higher end of the temperature and pressure range above 4.2–10 kbar and 530–800 °C, similar to estimates from dolerite dikes in the Kitak area. The syn-tectonic pegmatites with an intrusion age of 1843 ± 4 Ma formed corundum. The new data indicate that the pegmatite melt/fluid and the geotectonic setting are defining factors for generating plumasite-type corundum.

1. Introduction

Corundum (Al_2O_3) is a common accessory mineral in high-grade metamorphic terranes, and is interesting from a metamorphic, petrological and gemmological point of view. Corundum is colourless in its purest form, but traces of chromophores such as Fe, Cr, Ti, V, can colour corundum and form valuable gemstones of ruby and sapphire (Dubinsky et al. 2020). Most corundum deposits occur in orogenic belts or continental rift zones and formed in a metasomatic environment characterised by Al enrichment and Si depletion, and at temperatures above the gibbsite and diaspore stability field at > 400 to 450 °C (Feenstra 1985; Garnier et al. 2008; Giuliani et al. 2020; see Table 1). Aluminous protoliths include meta-sedimentary rocks, orthogneiss, syenite, anorthosite and pegmatite, whereas the low Si counterparts contain ultramafic rocks, basalt, amphibolite or marble (Simonet et al. 2008; Giuliani et al., 2014; 2020). Corundum in orogenic belts is formed at amphibolite

Abbreviations: AIC, Ammassalik Intrusive Complex; KTBU, Kap Tycho Brahe Unit.

* Corresponding author.
E-mail address: madp@geus.dk (M.D. Poulsen).

https://doi.org/10.1016/j.precamres.2022.106940
Received 28 September 2022; Received in revised form 30 November 2022; Accepted 1 December 2022
Available online 24 December 2022

to granulite-facies conditions during metamorphism and metasomatism (Simonet et al. 2008). Recent studies show that corundum formation is a predictable and often an integral part of the general geological history (e.g., Keulen et al. 2014; 2020, Yakymchuk & Szilas 2018, Giuliani et al. 2020; Hinsberg et al. 2021; Yakymchuk et al. 2021) resulting from the regional metamorphic, tectonic, and magmatic evolution. The metasomatic corundum formation requires contact and exchange of elements between two strongly contrasting rock types such as pegmatite and ultramafic rocks (plumasite-type, type IIB_1 after Giuliani et al. 2020), or external fluids interacting with a lithologitical suite e.g. the Fiskenæsset Anorthosite Complex (Aappaluttoq deposit, Keulen et al. 2014; 2020; Smith et al. 2016) or removal of volatile elements in closed system metamorphic *sensu stricto* reactions at amphibolite-granulite facies metamorphic conditions (Guiliani et al. 2020).

Corundum occurrences in Greenland outcrop in almost unweathered and well-exposed rocks (Garde & Marker 1988; Hinsberg et al. 2021; Keulen et al. 2014; 2020; Krebs et al. 2019; van Gool 2006; Yakymchuk & Szilas 2018), in contrast to most of the well-known localities worldwide that are heavily vegetated and deeply weathered or where corundum occurs in secondary deposits, e.g. as eluvial and colluvial placer deposits (Simonet et al. 2008). The Nattivit area is a unique site for a case study exploring plumasite-type corundum, which is exposed as primary deposit at only a few localities in the world including Plumas (California), Kenya, the Urals in Russia and Naxos in Greece (Lawson, 1903; Simonet 2000, Ishimaru et al. 2015; Voudouris et al. 2019; Guiliani et al. 2020), and nowhere with such excellent exposure. Corundum-bearing plumasite represent rocks that are the result of desilification of alkali-feldspar-bearing pegmatite bodies that intruded ultramafic rocks (Lawson 1903; Giuliani et al., 2014; 2020). Together with corundum, typically a thick layer of phlogopite and amphiboles are formed in a so-called black-wall (Simonet et al. 2008). Rather than only focussing on corundum formation, we use elemental and isotopic data, and U-Pb geochronology, to study the linkage between the plumasite-type corundum and the general geological history of the Nattivit area during the Paleoproterozoic Nagssugtoqidian Orogeny.

Here, we show the correlation between corundum formation and the overall crustal development in the Nattivit area during convergence, which are important driving forces for the corundum formation in the area. The composition and age of the basement that hosts the corundum was studied. Likewise, the geological processes in the region are of interest for understanding the Archean and Paleoproterozoic development of the region and other parts of the North Atlantic Craton, together with the timing between the crustal development and corundum formation. The new data from Nattivit area allow us to propose a genetic model for plumasite-type corundum.

Ruby and sapphire are gem variants of corundum, but most of the investigated material from the Nattivit area consists of raw material rather than cut and polished stones, of which it is harder to evaluate the quality. Most of the material appear as non-gem quality opaque stones and therefore the term 'corundum' is used throughout the text. The ultramafic rocks in the area are metamorphosed and their primary mineral phases have been partly altered, but the prefix 'meta' before the protolith names for the ultramafic rocks is omitted in the text.

2. Geological history of the Tasiilaq region

The Nattivit area is situated approximately 45 km SW of Tasiilaq in South-East Greenland (Fig. 1). The geology in the Tasiilaq region is defined by a 250 km wide SE-trending belt with Archean and Paleoproterozoic rocks (Bridgwater 1976; Kalsbeek, 1989; 1993) exposing the Nagssugtoqidian Orogen (Chadwick et al. 1989; Chadwick & Vasudev 1989, Kalsbeek 1989; Nielsen 1986; Nutman et al 2008; Kolb 2014). The rocks consist of TTG gneiss, metamorphosed mafic to ultramafic rocks (we will refer to the two rock types as (ultra)mafic rocks from here on in the text), metasedimentary units and syn-tectonic to post-tectonic intrusions.

Continent collision and formation of the Nagsugtoqidian Orogen has been proposed to stretch across the Kangerlussuaq-Aasiaat area in West Greenland to the Tasiilaq area in South-East Greenland. Correlation to other areas with collision at the same time period include the trans-Hudson Orogen in Canada, the Lewisian Complex in Scotland, the Svecofennian Orogen and Lapland Kola Orogen in Scandinavia (Wager and Hamilton, 1964; Palmer 1971; Tarney et al. 1972; Andrews et al. 1973; Wright et al. 1973; Myers, 1984; Myers 1987; Kalsbeek 1989; Bridgwater et al. 1990; Kalsbeek et al. 1993; Connelly et al. 2000; van Gool et al. 2002; Lahtinen et al. 2008; Nutman et al. 2008; St-Onge et al. 2009; Garde & Hollis 2010; Friend and Kinny, 2001; Kolb, 2014; Nicoli et al. 2017; Lebrun et al. 2018).

The Nagssugtoqidian Orogen is divided into three terranes, from south to north: the Isertoq, Kuummiut and Schweizerland Terranes (Kolb, 2014) (Fig. 1). The northern part of the Isertoq Terrane is intruded by three calc-alkaline, syn-tectonic intrusions, jointly called the Ammassalik Intrusive Complex (AIC) (Bridgwater, 1976; Chadwick et al. 1989; Kalsbeek et al. 1993; Nutman et al. 2008; Kolb, 2014; Kokfelt et al.

Table 1
Ruby deposit types and classification.

Geological setting	Magmatic		Metamorphic *sensu stricto*		Metamorphic - metasomatic		Sedimentary (placer)	
Metamorphic conditions	Amphibolite - granulite or eclogite facies		Greenschist - amphibolite -granulite facies		Greenschist - amphibolite - granulite facies		No metamorphism	
Type	I		II				III	
Subtype	A	B	A1	A2	B1	B2	A	B
Host rock /precursor	Alkali-basalt	Kimberlite	(ultra)mafic rocks	Marble and calc-silicate	Plumasite or metasomatite in (ultra)mafic rock or marble	structurally controled in gneiss, schist, (ultra)mafic	Alkali-basalt, kimberlite, lamprophyre	Metamorphic rocks
Deposits[a]	Antanifotsy, Soamiakatra, Madagascar	Mbuji-Mayi	Zimbabwe, South Africa, Tanzania, Madagascar, Ethiopia, Kenya, Malawi, Mozambique, France, Italy, Norway, Greece, Partkistan, India, New Zealand, Spain	Afghanistan, Nepal, Parkistan, Tajikistan, Myanmar, China, Vietnam, Tanzania, Kenya, Canada, Macedonia, Switzerland, France, Russia, Greece	South-Africa, Zimbabwe, Kenya, Tanzania, Madagascar, Russia, Australia, United States, France, Greenland, India, Russia	Madagascar, India, Kenya, Tanzania	Australia, China, Thailand, Cambodia, Madagascar, Kenya, Democratic Republic of Congo, Brazil	Sri Lanka, Myanmar, Vietnam, Tanzania, Mozambique, Malawi, United States

[a] see Giuliani et al. 2020 for details on the different deposits.

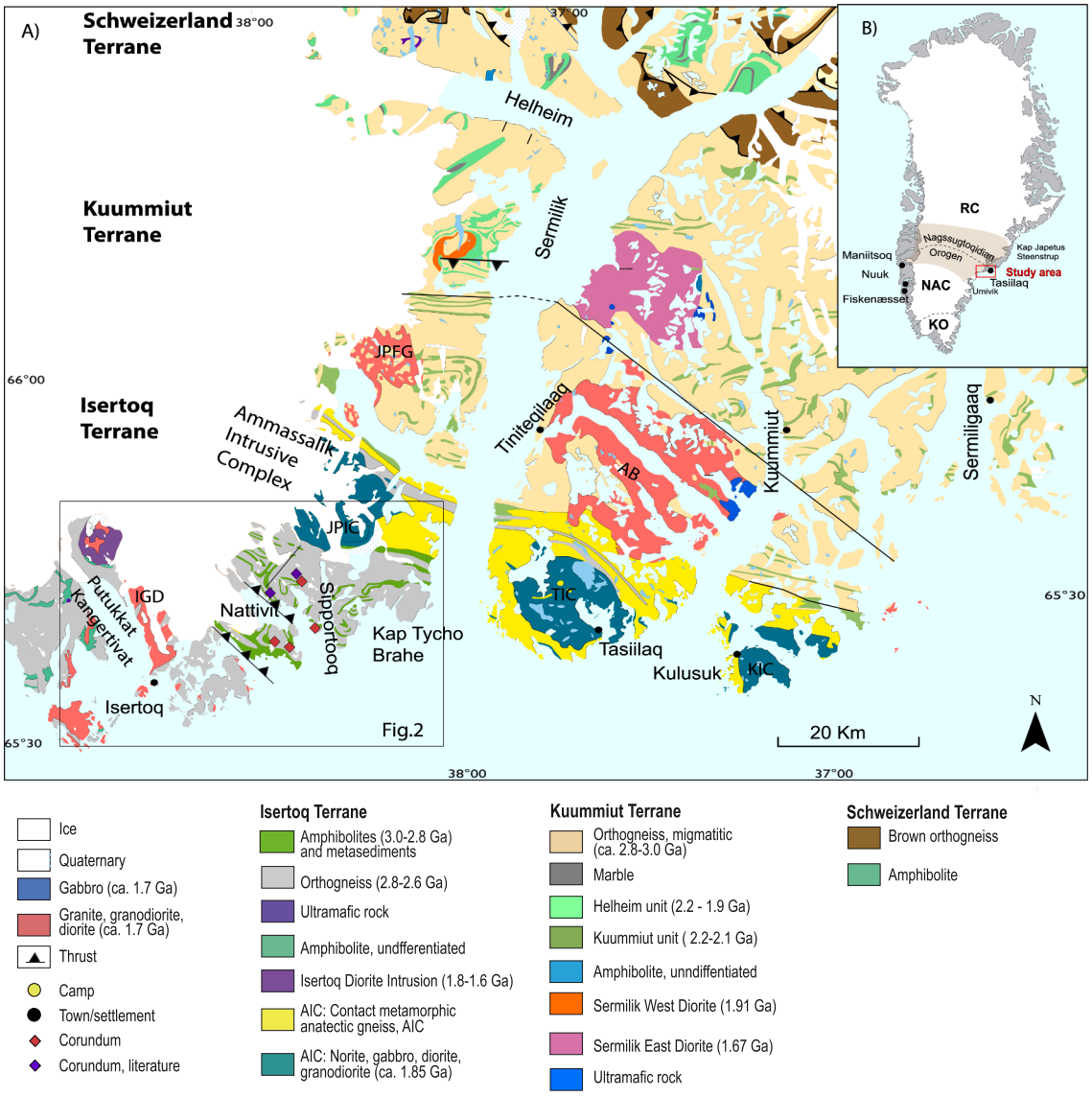

Fig. 1. A) Geological map of the Tasiilaq area in South-East Greenland modified after Escher (1990), Pedersen et al. (2013), Kolb (2014). Abbreviations are: JPIC = Johan Petersen Intrusive Centre, TIC = Tasiilaq Intrusive Centre, KIC = Kulusuk Intrusive Centre, AB = Ammassalik Batholith, JPFG = Johan Petersen Fjord Granite, IGD = Isertoq granites and diorites, AIC = Ammassalik Intrusive Complex. B) Inset map of Greenland indicating the location of the Tasiilaq area in South-East Greenland (red square). The main localities with corundum occurrences in West Greenland are also marked (Maniitsoq, Nuuk and Fiskenæsset). NAC = North Atlantic Craton, RC = Rae Craton, KO = Ketilidian Orogen. The boundary between the cratons are marked with dashed line and the extend of the Nagssugtoqidian Orogen is highlighted. (For interpretation of the references to colour in this figure legend, the reader is referred to the web version of this article.)

2016b; Lebrun et al. 2018). The Kuummiut and Schweizerland Terranes are part of the Rae Craton (Nutman et al. 2008; Kolb, 2014; Nicoli et al. 2017; Müller et al. 2018a, b), whereas the Isertoq Terrane is part of the North Atlantic Craton (NAC; Kolb, 2014). The NAC acted as the upper plate during convergence and continent collision in the Nagssugtoqidian Orogeny (1910–1840 Ma) (Kolb 2014; Müller et al. 2018a), with the Schweizerland Terrane thrust on top of the Kuummiut Terrane. The maximum extent of deformation related to the Nagssugtoqidian Orogen in South-East Greenland streches from Umivik in the south to Kap Japetus in the north (Fig. 1B) (Dawes et al., 1989; Escher et al. 1989; Bridgwater et al. 1990).

The terranes all expose meso- to Neoarchean basement of predominantly TTG gneiss and lesser amphibolite (Wright et al. 1973; Myers 1984; 1987; Kalsbeek 1989; Kalsbeek et al. 1993; Nutman et al. 2008; Kolb 2014; Kokfelt et al. 2016a, b, c; Müller et al. 2018a). Metasedimentary sequences are also common, including meta-semi-pelite, paragneiss, quartzite and calc-silicate rocks, as are ultramafic rocks and diorite to monzogranite intrusions (Wright et al. 1973; Hall et al., 1989b; Bridgwater et al. 1990; Kalsbeek et al. 1993; Nutman et al. 2008; Kolb et al. 2016; Thrane et al. 2016; Nicoli et al. 2017; Müller et al. 2018a; Lebrun et al. 2018). Four deformation stages related to the Nagssugtoqidian Orogeny are identified from WSW-vergent subduction and ENE-trending shear zones (D_1) to continent collision (D_2) and strike-slip movement, block juxtaposition (D_3) with a SW-vergent thrust and ramp system, and finally (D_4) post-orogenic extension in a NE-SW direction with monzogranite to diorite intrusions (Kolb, 2014).

Post-tectonic intrusions include monzogranite, diorite and gabbro intruded from 1.67 to 1.52 Ga (Thrane et al. 2016). The intrusions include the Ammassalik Batholith north of Tasiilaq, the Sermilik East and West Diorites, the Johan Petersen Fjord Granite and the Isertoq granites and diorites (Kokfelt et al. 2016b; Thrane et al. 2016) (Fig. 1).

2.1. The Isertoq Terrane

The study area is centred on the Nattivit Kangertivat fjord which is part of the Isertoq Terrane (Fig. 1, 2). The Isertoq Terrane is composed of TTG gneiss, amphibolite, ultramafic rocks, mica schist, quartzite, monzogranite, diorite, pegmatite and lesser amounts of calc-silicate rocks (Wright et al. 1973; Chadwick et al. 1989; Hall et al. 1989a; Kolb 2014). TTG gneiss dominates and varies from well-foliated to massive, fine- to coarse-grained, with local migmatisation (Wright et al. 1973). Archean TTG gneiss close to Isertoq has U-Pb zircon intrusion ages of 2822 ± 8 Ma and 2724 ± 4 Ma (Kokfelt et al. 2016a). On Kitak island and west of the Isertoq diorite, boudins of anorthosite/leucogabbro are present in 2758 Ma ± 4 Ma TTG gneiss (Nunes et al. 1974; Kokfelt et al. 2016a).

Meta-sedimentary rocks characterise the Paleoproterozoic stage in the Isertoq Terrane. They tectonically overlie the Archean TTG gneiss and an (ultra)mafic sequence that Bridgwater & Gormsen (1968) interpreted to be Paleoproterozoic. The tectonostratigraphy of the (ultra)mafic and metasedimentary sequence was first described by Wright et al. (1973), Hall et al. (1989a), Chadwick et al. (1989) and defined by Chadwick & Vasudev (1989) as the Síportôq Supracrustal Association. This was subsequently modified by Kolb (2014) into the Kap Tycho Brahe Unit (KTBU). The KTBU ranges between 200 m and 1

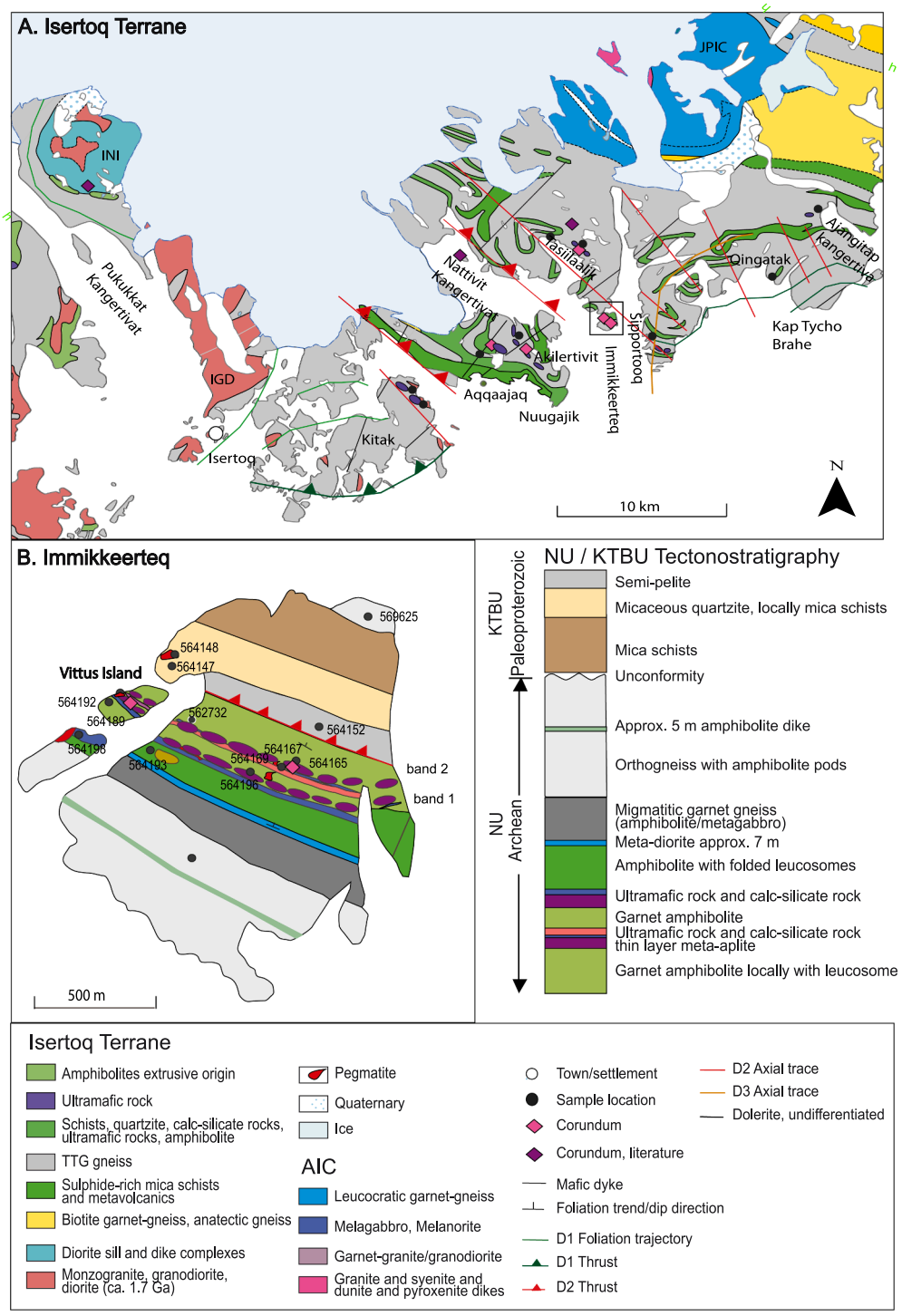

Fig. 2. A) Geological overview map of the study area in the Isertoq Terrane, modified after Stensgaard et al. (2016), and structures are from Kolb (2014). B) Detailed geology of the Immikkeerteq island with a tectonostratigraphic section. Abundant corundum occurrences are present in the study area associated with metasomatic interaction of pegmatites with ultramafic rocks. Abbreviations are NU= Nattivit Unit, KTBU= Kap Tycho Brahe Unit, AIC= Ammasalik Intrusive Complex. (For interpretation of the references to colour in this figure legend, the reader is referred to the web version of this article.)

km in thickness and consists of four amphibolite units separated by two bands of ultramafic rocks and thin calc-silicate rock bands overlain by micaceous quartzite, metapelite and semipelite next to amphibolite (Fig. 2b) (Hall et al. 1989a). According to Wright et al. (1973), the ultramafic rocks range in composition from dunite to lherzolite and include pyroxenite with large enstatite grains up to 3 cm in size, where their formation is suggested to be metasomatic (Wright et al. 1973). A quartzite from Immikkeerteq island was described by Wright et al (1973) showing trough-bedding with way-up criteria younging towards NW. Thrust sheets of the KTBU and TTG gneiss are tectonically interleaved in a layer cake structure in the Isertoq Terrane (Chadwick et al. 1989) and imbricated from a SE-vergent thrust and ramp system (Kolb, 2014). A biotite-garnet paragneiss adjacent to the AIC gives U-Pb zircon age peaks at 2067 ± 13 Ma, 1985 ± 10 Ma and 1902 ± 10 Ma (Lebrun et al. 2018). A paragneiss close to the Isertoq settlement gives U-Pb zircon age peak at 1937 ± 7 Ma (Thrane et al. 2016), and a mica schist from the Nattivit area includes dates from 2050 to 1900 Ma with a smaller peak around at 2150 Ma (Thrane et al. 2016).

The northern part of the Isertoq Terrane hosts the AIC (Fig. 1). The AIC is composed of mafic to intermediate rocks (norite, gabbro, diorite, granodiorite, monzogranite) and has been emplaced in three magmatic pulses between 1910 and 1870 Ma (Lebrun et al. 2018). The AIC intrusions are interpreted to be either derived from magma originating from the upper mantle or subcontinental lithosphere that intruded during subduction of the Kuummiut Terrane below Isertow Terrane or formed from anatectic melts from garnet-bearing host rocks (Lebrun et al. 2018).

Peak metamorphic conditions for the Isertoq Terrane are upper amphibolite to granulite facies (e.g. Kolb 2014). Nutman & Friend (1989) report peak conditions of 650–660 °C and 7 to 8.5 kbar for a garnetiferous dike from Kitak. Rocks adjacent to the AIC show contact metamorphism at 710–780 °C at 7.5 kbar as constrained from orthopyroxene-garnet thermometry (Nutman & Friend 1989).

Pegmatites are abundant, and multiple, cross-cutting generations are commonly observed. They range between granitic to anorthositic in composition, are often distinct in mineralogy, grain size and orientation, suggesting that they represent multiple generations. Locally, interaction between pegmatite and ultramafic rocks formed metasomatic corundum (Hall et al. 1989a, Poulsen et al. 2015).

3. Materials and methods

Fieldwork was conducted in the area between Putukkat Kangertivat and Kap Tycho Brahe (Fig. 2) in 2014 and 2015 from four land-based camps, using boat and helicopter support. The purpose of the fieldwork was to map the geology in selected areas, with emphasis on the lithologies hosting corundum and their enclosing units, of the broader perspective of the regional geology, and for collecting key samples of TTG gneiss, paragneiss, quartzite, mica schists, pegmatite, amphibolite, meta-gabbro and ultramafic rocks for bulk rock elemental and isotopic analyses (including zircon dating) to determine protoliths (see Table 2, S1 and a more detailed description on the methods in the supplementary file 1).

A detailed transect of the KTBU rocks was studied on Immikkeerteq island and the small islets surrounding it, which expose an approximately 1 km thick tectonostratigraphic sequence of the KTBU, that hosts abundant plumasite-type corundum occurrences, in order to obtain a better documentation of these rocks (Table 2). A total of 32 samples were analysed for whole-rock major elements and a subset of 21 samples also for trace elements. These samples include amphibolite, meta-gabbro, ultramafic rock, and felsic schists. Ten samples were analysed for Sm-Nd, Rb-Sr and Pb-Pb isotopic compositions using a VG Sector 54 IT Thermal Ionisation Mass Spectrometer (TIMS) at the University of Copenhagen at the Department of Geosciences and Natural Resource Management in Denmark (IGN). The purpose of the radiogenic isotope analyses was to constrain the age of the (ultra)mafic rocks and to test continental crust influence on the (ultra)mafic rocks.

Scanning Electron Microscopy (SEM) analyses were performed with the ZEISS Sigma 300 VP field emission SEM at the Geological Survey of Denmark and Greenland (GEUS), which is equipped with a back scattered electron (BSE) detector, two energy dispersive spectrometers (EDS) and a cathodoluminensce detector. Mineral compositions were determined using a JEOL JXA-8200 Superprobe at IGN at the University of Copenhagen. Ten samples, including pegmatite, paragneiss, quartzite and TTG gneiss, were dated by zircon U-Pb geochronology using laser ablation inductively coupled plasma mass spectrometry (LA-ICP-MS) (Table S1). The purposes for dating these different lithologies were to constrain the timing of protolith formation, of orogeny, and the timing of plumasite formation.

4. Results

4.1. Field observations in the Isertoq Terrane and samples

The study area is dominated by felsic to intermediate TTG gneiss and (ultra)mafic rock, where the meta-sedimentary lithologies (quartzite, meta-pelite, mica schists, quartzite) structurally overlie the TTG gneisses and the (ultra)mafic rocks (Figs. 2, 3). The TTG gneiss and (ultra)mafic rock sequence from the KTBU are intruded by syntectonic and post-orogenic mafic to felsic intrusions of noritic, monzodioritic and granitic compositions, and pegmatite dikes. On Immikkeerteq island (Fig. 3A), a fault is observed at the northern end of the island where Paleoproterozoic meta-sedimentary rocks are in direct contact with the Archean rocks. The KTBU is tectonically repeated multiple times in the Isertoq Terrane.

4.1.1. Amphibolite

Amphibolites occur as lenses and boudinaged layers in the Archean TTG gneiss and large units thicker than 10 m. Relative age relations between TTG gneiss and amphibolite is not always straightforward because the primary contacts are modified. The large units of amphibolite found in the Kap Tycho Brahe Unit have a sharp contact with the TTG gneiss on the southern end of the Immikkeerteq island. These amphibolite units are thick and more continuous compared to the lenses in the TTG and reach up to 600 m thickness on Immikkeerteq island (Fig. 3A). However, in multiple locations around the Isertoq diorite complex, field observations indicate that amphibolite was intruded by TTG and folded together in later deformation, and hence the mafic rocks pre-date the Archean TTG intrusion. The amphibolites at Tasiilaalik are well-foliated and isoclinally folded and are cut by TTG dikes at a shallow angle to the overall foliation. It appears that these TTG gneisses were parallelised in a later deformation event. Field observations at Tasiilaalik likewise show one type of amphibolite has an additional foliation compared with other amphibolite in the area, which indicates they may be Archean. On Immiikkeerteq the amphibolite belonging to the Archean group were studied in more detail; here four slightly different amphibolite types are distinguished: Starting from the N of the island at the thrust fault working towards S, the first type of amphibolite is fine-grained, often strongly foliated, with large coherent leucosomes parallel to the foliation and smaller melanosomes. The second type is a medium- to coarse-grained garnet amphibolite (Fig. 4A, sample 564193) with 1–3 cm sized garnet porphyroblasts. The third is medium-grained with folded plagioclase-quartz veinlets (sample 564192). These commonly show malachite staining on joints. The fourth type is a garnet-bearing, dark grey amphibolite/meta-gabbro with folded migmatitic veins containing both felsic and mafic parts. The main foliation trends NW-SE and dips ~ 35-60°NE. The essential minerals in the amphibolite from the garnet amphibolite measured with SEM-EDS are hornblende, plagioclase and quartz, with smaller amounts of garnet, diopside, biotite, carbonate, epidote, microcline and minor titanite.

The younger amphibolite generation could represent metamorphosed dikes/sills as observed on the Immikkeerteq island, where a

Table 2
Sample list and indications for the applied analytical techniques for the samples from Isertoq Terrane (this study).

Sample No	Locality	Latitude	Longitude	Rock type	Minerals	SEM-EDS[a] Method	XRF[b] Method	ICP-MS[c] Method	EMPA[d] Method	LA-ICP-MS[e] Method	TIMS[f] Method
562732	Immikkeerteq	65.6208	−38.4844	Lherzolite	Opx, Chr, Ilm, Ath, Act, Srp, Phl, Chl		x	x	x		x
562741	Immikkeerteq	65.6195	−38.4815	Lherzolite	Opx, Ath, Act, Chl, Chr, Dol, Ap, Pn, Phl, Ilm		x				
569204	Kuummiut	65.8823	−36.9876	Lherzolite	Opx, Ol, Ath		x	x			
564111	Aqqaajaq	65.5990	−38.6285	Orthogneiss	Bt, Fsp, Qz, Tsr					x	
564115	Aqqaajaq	65.5985	−38.6311	Dunite	Ol, Opx, Ath, Srp, Pn		x	x			
564116	Aqqaajaq	65.5984	−38.6311	Dunite + crn	Tsr, Crn, Pl, Ru, Ap	x			x		
564119	Aqqaajaq	65.5984	−38.6330	Dunite	Ol, Opx, Ath, Srp, Pn			x			
564125	Aqqaajaq	65.5998	−38.6265	Mica schist	Qz, Pl, Bt, Zrn, Ilm	x	x		x		
564128	Aqqaajaq	65.6025	−38.6349	Dunite + Crn	Bt, Amp, Crn	x			x		
564129	Aqqaajaq	65.6025	−38.6349	Dunite	Ol, Opx, Ath, Srp, Chl, Tlc, Pn	x	x	x	x		
564130	Aqqaajaq	65.6023	−38.6345	Dunite + Crn	Crn, Pl, Tsr	x		x			
564133	Aqqaajaq	65.6023	−38.6345	Dunite	Ol, Opx, Ath, Srp, Pn		x	x			
564135	Aqqaajaq	65.6013	−38.6379	Dunite + Crn	Crn, Pl, Tsr						
564139	Aqqaajaq	65.6010	−38.6346	Dunite	Ky, Tsr, Pl, Ap, Ba-Fsp, Or, Phl, Ath	x					
564140	Aqqaajaq	65.6010	−38.6203	Schist/aplite	Pl, Or, Ms, Qz, Bt, Gt, Ap	x	x		x		
564143	Aqqaajaq	65.6005	−38.6234	G1 pegmatite	Qz, Fsp, Bt, Pl					x	
564147	Immikkeerteq	65.6222	−38.4820	Quartzite	Amp, Qz, Fsp, Mcl, Ms, Bt					x	
564148	Immikkeerteq	65.6225	−38.4815	G1 pegmatite	Bt, Ms, Qz,					x	
564152	Immikkeerteq	65.6222	−38.4655	Paragneiss-metasemi-pelite	Qz, Bt, Amp, Fsp					x	
564156	Immikkeerteq	65.6185	−38.4726	Lherzolite	Tc, Chr, Phl, Pn, Py, Dol, Ath	x	x	x			
564165	Immikkeerteq	65.6181	−38.4712	G2M Pegmatite	Pl, Fsp, Amp					x	
564167	Immikkeerteq	65.6181	−38.4712	Lherzolite	Opx, Chr, Hbl, Act, Ath, Phl, Chl, Dol	x	x	x	x		
564168	Immikkeerteq	65.6181	−38.4712	Calc-silicate	Phl, Chr, Ath, Act, Tlc, Chl	x					
564169	Immikkeerteq	65.6181	−38.4712	Meta-aplite	Phl, Qz, Ap, Ba-Fsp, Or, Zrn	x					
564178	Tasiilaalik	65.6726	−38.5345	Dunite	Opx, Ath, Ol, Srp		x	x			
564179	Tasiilaalik	65.6726	−38.5345	G2 Pegmatite	Pl, Qz, Bt, Pl		x				
564180	Tasiilaalik	65.6731	−38.5347	Lherzolite + Crn	Ky, Crn, Hbl, Bt-Phl, Ba-Fsp, Or, Pl, Zrn, Tsr	x					
564182	Tasiilaalik	65.6731	−38.5347	Lherzolite	Ath, Srp, Opx		x	x			x
564185	Vittus island	65.6211	−38.4855	Lherzolite + Crn	Crn, Tsr, Bt, Or, Dol, Pl, Zrn, Py, Fc, Act	x			x		
564188	Vittus island	65.6211	−38.4855	Calc-silicate rock	Ba-Fsp, Act, Bt, Or, Pl, Zrn, Qz	x					
564189	Vittus island	65.6211	−38.4855	G2 Pegmatite	Pl, Qz, Bt	x	x			x	
564190	Vittus island	65.6211	−38.4855	Lherzolite	Opx, Ath, Act, Chl, Chr, Dol, Ap, Pn, Phl, Ilm	x	x	x	x		
564192	Vittus island	65.6210	−38.4862	Amphibolite	Hbl, Qz, Fsp, Pl, Bt		x	x			x
564193	Vittus island	65.6137	−38.5900	Gt amphibolite	Bt, Qz, Gt, Hbl, Or, Pl	x	x		x		
564196	Immikkeerteq	65.6190	−38.4799	Lherzolite	Opx, Ath		x	x			x
564198	Vittus island	65.6200	−38.4891	Gt mica schist	Gt, Bt, Or, Zrn, Cal, Qz, Ttn, Ep, Ab, Fsp, Py, Ccp	x	x		x		
564199	Vittus island	65.6726	−38.5345	Orthogneiss	Qz, Bt, Fsp, Amp, Mcl					x	
569601	Akilertivit	65.6049	−38.5742	Lherzolite + Crn	Tsr, Crn, Pl, Ap		x	x			x
569602	Akilertivit	65.6049	−38.5742	Dunite	Pl, Ol, Ath, Ap, Opx		x	x			x
569603	Akilertivit	65.6131	−38.5895	Dunite	Ath, Opx		x	x			x
569607	kitak	65.5805	−38.7568	Lherzolite	Ath, Opx		x	x			
569611	Kitak	65.5795	−38.7579	Lherzolite	Ath, Opx		x	x			x
569618	Sipportooq	65.5950	−38.4112	Lherzolite	Opx, Amp		x	x			x
569621	Ajangitap k.[g]	65.6952	−38.1867	Lherzolite	Fsp, Qz, Mc, Bt		x	x			
569624	Qingatak	65.6558	−38.2772	Meta-gabbro	Ol, Pl, Amp, Pl		x	x			x
569625	Immikkeerteq	65.6254	−38.4660	Orthogneiss	Amp, Bt, Fsp, Qz					x	
569628	Tasiilaalik	65.6753	−38.5656	G3 Pegmatite	Fsp, Bt, Qz, Bt					x	
569632	Kitak	65.5667	−38.7252	Ilmenite vein	Ilm		x	x			
569633	Kitak	65.5667	−38.7252	Lherzolite	Ath, Opx, Dol, Srp,		x	x			x

[a] Mineral composition.
[b] Major element.
[c] Trace elements.
[d] Mineral composition.
[e] U/Pb zircon dating.

[f] Rb-Sr,Pb-Pb Sm-Nd isotope.
[g] Ajangitap kangertiva.

5 m wide lense in TTG gneiss is observed (Fig. 2). However, this deformed dike appears to have been folded with the TTG and is thus older than the Nagssugtoqidan deformation. A greenish, olivine-rich meta-gabbro from Qingatak (sample 569624) is enclosed by TTG gneiss. From field observation it is unclear where the meta-gabbro fits in the overall stratigraphy. Late dolerite dikes trending NE/SW are observed in the area around Kitak and Aqqaajaq, cross-cutting the TTG gneiss, amphibolite and ultramafic rocks (Fig. 3B). These dikes only show slight foliation. The dolerites are red brown for the coarser grained types and observed to be up to 20 m wide, and the thin dikes, less than 0.5 m wide, are finer grained and black. The dike cross-cutting the Nattivit kangertivat (Fig. 2) is coarse-grained, weathers red brown, is strongly magmatic and contains visible minerals of pyroxene, magnetite and garnet.

4.1.2. Ultramafic rocks sensu lato

Ultramafic rocks in the Isertoq Terrane are a minor constituent and occur predominantly as lenses in amphibolite of the Kap Tycho Brahe Unit, and to a lesser extent in TTG gneiss. The ultramafic lenses in the TTG gneiss are small and up to 1 m. The ultramafic lenses in the Kap Tycho Brahe Unit are up to 100 m wide and 500 m long (Fig. 3A, 3B). The ultramafic rocks have been partly altered and the rocks are therefore referred to as ultramafic rock *sensu lato*. From field observations it appears there are two slightly different groups of ultramafic rocks. The first group is a metamorphosed lherzolite, or alternatively orthopyroxenite or harzburgite. However, the ultramafic rock type was obscured from field observations alone. The second group appear as metamorphosed dunite or harzburgite.

The first group observed at Immikkeerteq, Vittus island, Kitak, Tasiilaalik, Sipportooq are the metamorphosed lherzolite/orthopyroxenite/harzburgite. The ultramafic rock consists of brown, massive, unfoliated, medium- to coarse-grained rock that contains enstatite (some outcrops have 1–3 cm diameter porphyroblastic enstatite), augite and minor dolomite, chromite, anthophyllite, actinolite, antigorite and chlorite.

Two parallel bands of boudinaged ultramafic rocks are traced from Vittus island accross Immikkeerteq to Sipportooq (Fig. 3A). The individual boudins crosscut the foliation and the tectonostratigraphic layering at a shallow angle, indicating an intrusive relationship. Between the ultramafic rock and the host amphibolite there is a fine-grained metasomatic hornblende-rich black-wall contact at one side and a calc-silicate-rich layer to the other contact.

The second group are the metamorphic dunite, or alternatively a harzburgite, and observed at Aqqaajaq, Akiletivit and Tasiilaalik. There are two approximately 5 m wide bands of boudinaged dunite bands exposed at Aqqaajaq and Akilertivit, as well as a large body of approximately 0.5 km^2 (Fig. 3B). The rocks are fine-grained, redbrown and composed of enstatite, olivine, phlogopite, minor pyrite, apatite, anorthite, carbonates, antigorite and chlorite (Fig. 4B). The high antigorite content indicates the ultramafic rocks are metamorphosed dunite. The dunite at Akilertivit appears to be related to the larger dunite body at Aqqaajaq. The ultramafic rocks at Tasiilaalik also occur in two bands, where one band is identified as a dunite and the other as lherzolite/orthopyroxenite/harzburgite.

4.1.3. Orthogneiss

The TTG gneiss are equivalent to the descriptions of grey TTG gneiss in the area by Wright et al. (1973). The TTG gneisses comprise quartz, oligoclase, and variable amounts of biotite and hornblende. The TTG gneiss contains bands, seams, boudins and lenses of pegmatite, amphibolite, anorthosite or diopside-rich rocks (Fig. 3C), which range in size from under a metre to tens of metres, and commonly can be traced along strike. At Aqqaajaq, a light-coloured well banded and folded TTG gneiss was observed at the contact to amphibolite and ultramafic lenses. The minerals observed in the orthogneiss are plagioclase, biotite and quartz, and a foliated light-coloured TTG gneiss at Tasiilaalik has gradational changes to a mafic mineral mode where the leucocratic parts contain feldspar and the mafic parts contain plagioclase, amphibole and biotite. These TTG gneisses are in direct contact to amphibolite with ultramafic boudins and indicate an intrusive relationship into the amphibolites. A third type of TTG gneiss is compositionally heterogeneous, with felsic pegmatitic parts (Fig. 3C) containing quartz, biotite and lesser amounts of pink feldspar, while the mafic parts contain biotite, amphibole, plagioclase and quartz. The pegmatitic orthogneiss is in contact with the mica schists on Immikkeerteq and contains boudins of amphibolite and diopside-rich lenses.

4.1.4. Calc-silicate rocks

Horizons of calc-silicate rocks are present throughout the area. On Immikkeerteq and surrounding islets, calc-silicate rocks are found as a light-green andradite-epidote gneiss (Fig. 3N, sample 564198) with 2–5 cm sized porphyroblastic, mauve-coloured andradite in a groundmass of epidote, biotite, quartz, titanite, calcite, dolomite and feldspars (hyalophane, orthoclase, albite). An approximately 2 m thick sequence of green, foliated and boudinaged calc-silicate rock (sample 564188) comprises green augite and actinolite, phlogopite-biotite, feldspar (hyalophane, andesine, orthoclase) and minor quartz. Likewise, a thin layer (0.5–1 m wide) of whitish, greenish or purplish horizons of calc-silicate rock, is in contact with the ultramafic boudins (sample 564168). The latter contain diopside, actinolite, epidote, calcite, and minor green mica and garnet. Large sequences of light to dark green often strongly folded calc-silicate rocks were observed at Nuugajik.

4.1.5. Mica schist and quartzite

The mica schists are rusty-red, banded, coarse-grained and contain garnet, quartz, feldspar, biotite ± muscovite, and minor blue kyanite/sillimanite, graphite and pyrite. A garnet mica schist at Aqqaajaq (sample 564125), has a high mode of almandine garnet in a matrix of quartz, oligoclase, biotite, and minor zircon and ilmenite with leucosomes of quartz and feldspar. A similar garnet mica schist on Immikkeerteq is 4 m thick, well-foliated and coarse-grained, and occurs adjacent to a meta-diorite. It contains garnets up to 2 cm in size, quartz and plagioclase and has rusty patches related to minor interstitial sulfides. An intensely folded metasemipelite (or paragneiss) is present at the highest point of Immikkeerteq island (sample 564152). The metasemipelite has varying layers of light to greyish colours with slight variations in quartz, biotite and feldspar contents. A quartzite unit is present on the northern end of the island, which is light coloured and consists of up to 85 % quartz. The remaining minerals are plagioclase and muscovite (Fig. 3D, sample 564147).

4.1.6. Pegmatite and post-tectonic felsic intrusions

Small pre- or syn-tectonic intrusive bodies (1–7 m thickness) are observed foliation parallel to the Kap Tycho Brahe Unit amphibolite and include diorite and one aplite on Immikkeerteq and Aqqaajaq. The mineral assemblage is oligoclase, orthoclase, muscovite, quartz, biotite, and minor almandine garnet, biotite and apatite.

Three generations of felsic pegmatites have been identified. The oldest pegmatites (Group 1) are folded and show tight isoclinal folds at Aqqaajaq and open or symmetrical folds at Immikkeerteq and Qingatak, and are pre- to syn-tectonic intrusions. The width of the Group 1 pegmatite is up to 1 m. The second group (Group 2) pegmatites are often wide - up to 15 m thick, pink in colour and have a high feldspar content (microcline and plagioclase), with less than 15 % quartz and biotite (Fig. 3E). They are syn-tectonic intrusions and strike NE/SW. One of the Group 2 pegmatites has an offshoot that crosscuts Vittus island and

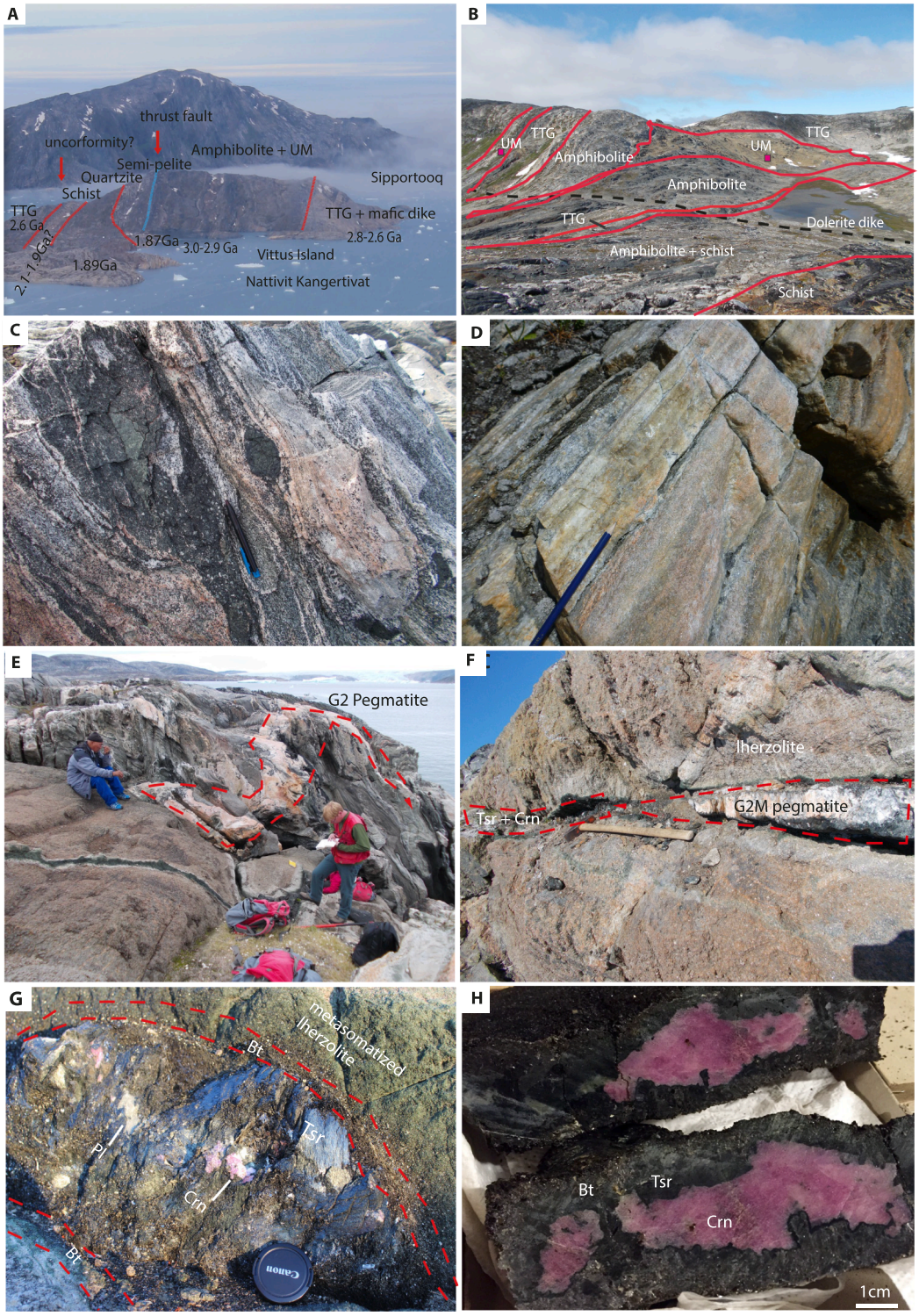

Fig. 3. Field observations in the Isertoq Terrane: A) Immikkeerteq island seen from the inner part of Nattivit kangertiva. B) Aqqaajaq with ultramafic rock outcrop, where the different rock types are indicated with red lines. C) TTG gneiss (569625) from Immikkeerteq with lenses of amphibolite and ultramafic rocks. D) The quartzite (564147) on Immikkeerteq. E) Brown ultramafic rock on Vittus island and intrusion of (Group 2) pegmatite (sample 564189) which formed a corundum vein. F) A desilicified pegmatite (Group 2M) crosscutting an ultramafic rock lense at Immikkeerteq and formation of corundum. G) Reaction zone from Vittus island where Group 2 (564189) pegmatite has reacted with the ultramafic rock. The reaction zone shows concentric arrangement around the intrusion of the pegmatite with metasomatized ultramafic rocks and layers of biotite and in the center amphibole and corundum. H) A vein of pure corundum and tschermakite. (For interpretation of the references to colour in this figure legend, the reader is referred to the web version of this article.)

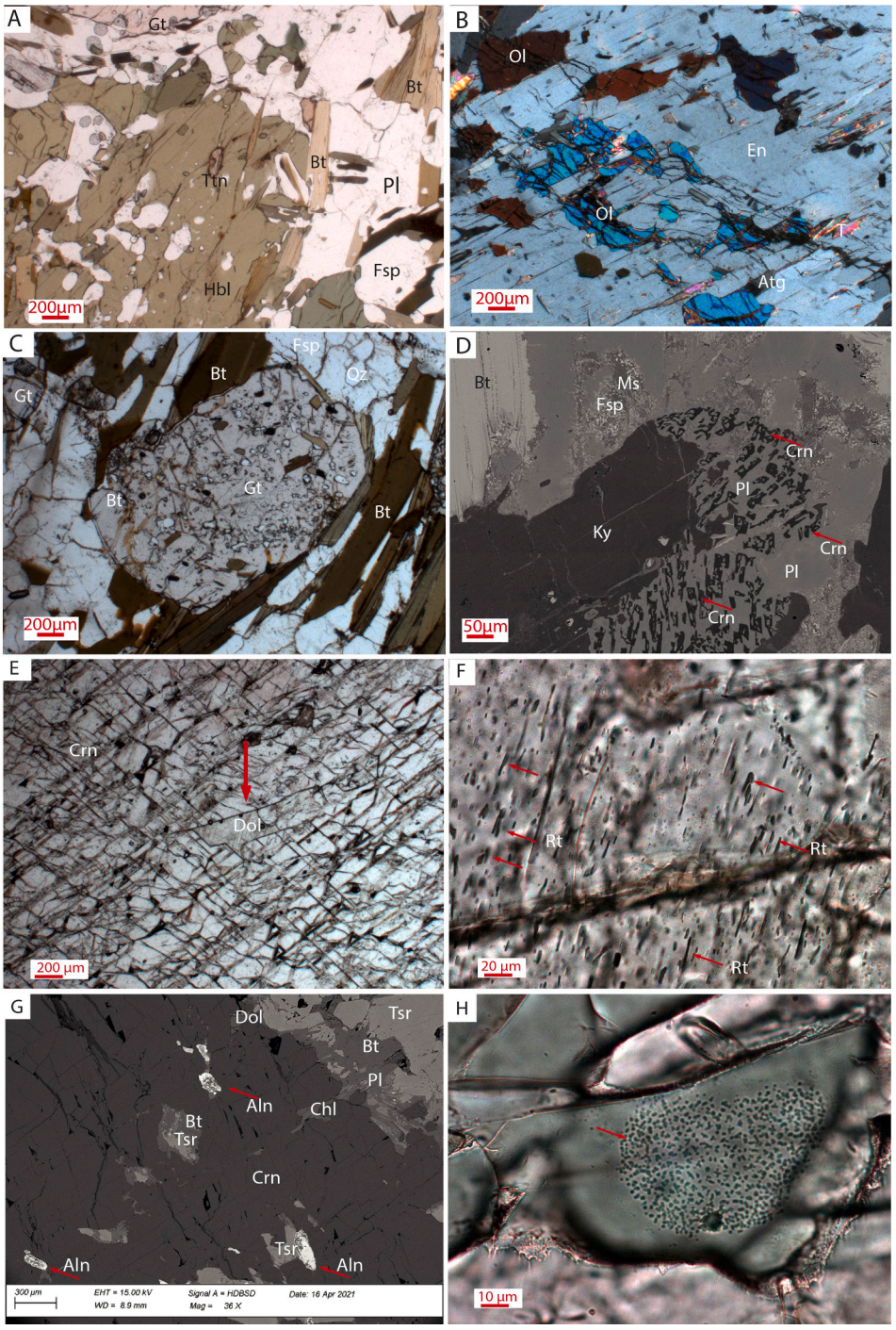

Fig. 4. Petrographic examination in Plain Polarized Light (PPL) and Crossed Polarized Light (XPL), as well as Back-Scatter Electron (BSE) images of selected rocks in thin sections. A) Garnet amphibolite (564193) in PPL. B) Dunite 564129 in XPL. C) Garnet mica schist (564125) in PPL. D) BSE image of corundum, placioclase and kyanite (564180) in metasomatic reaction zone in lherzolite. E) Heavily fractured corundum with dolomite grain in the centre of the photo (564185) in PPL. F) Rutile needles in corundum (564185) in PPL. G) BSE image of inclusions in the corundum including allanite, tschermakite, biotite and dolomite (564185). H) Cloud of small inclusions in corundum hosted in dunite (564116) in PPL. The corundum is heavily fractured. Mineral abbreviation are after Warr (2021): Aln = allanite, Atg = antigorite, Bt = biotite, Cal = calcite, Chl = chlorite, Crn = corundum, Dol = dolomite, En = enstatite, Fsp = feldspar, Gt = garnet, Hbl = amphibole, Ilm = ilmenite, Ky = kyanite, Ol = olivine, Pl = plagioclase, Qz = quartz, Rt = rutile, Tsr = tschermakite. Ttn = titanite. (For interpretation of the references to colour in this figure legend, the reader is referred to the web version of this article.)

reacts with the ultramafic rocks on the island, and can be traced onto Immikkeerteq island (sample 564189) and is associated with corundum on Vittus island. The desilicified version of Group 2 pegmatite is labelled as Group 2M, where M indicates metasomatic alteration. These pegmatites are progressively desilicified upon reaction with the ultramafic rocks (Fig. 3F). They are silica-poor and more intermediate in composition with a high plagioclase content. The minerals in the desilicified pegmatites include anorthite, albite, orthoclase, muscovite-biotite, calcite, clinochlore, apatite and zircon (sample 564165).

The pegmatites of the third group (Group 3) are wide and pale, with high (orthoclase) feldspar contents, and with a NE-SW to N-S strike (sample 569628). The width of the Group 3 pegmatites is up to 10 m at Kitak. They crosscut the Group 2 pegmatites e.g. at Tasiilaalik and crosscut the post-tectonic Isertoq granites at Kitak. They often show graphic texture, and are very coarse-grained with mineral grains up to 3–5 cm. No corundum related to Group 3 pegmatite was observed. The desilicified pegmatites derived from Group 3 are named Group 3 M and contain feldspar, apatite and ilmenite.

Post-tectonic intrusions include large intrusive sheets of undeformed monzogranite and diorite that dominate around Isertoq (approximately 60 km^2) and towards Putukkut kangertivat. The exposed part of the intrusive complex in Putukkut kangertivat covers an area of approximately 25 km^2 and consists of ~ 80 % diorite and ~ 20 % granite. The intrusion complex has a dome-like structure and intrudes into the amphibolite and orthogneiss. Mingling textures between a fine-grained, dark-grey diorite and a light-grey, medium-grained diorite indicate

multiple magma pulses while the rocks were still partly molten. The granite is very light-coloured and consists of plagioclase, alkali feldspar, quartz, and minor amphibole and biotite. The granite contains abundant rafts of diorite, which suggests that the diorite had cooled sufficiently before intrusion of the granite melt. The intrusive sheets have been dated at 1.7–1.5 Ga (Thrane et al. 2016).

4.1.7. *Corundum occurrences in ultramafic rocks*

Corundum occurrences in ultramafic rocks are found at Aqqaajaq, Tasiilaalik, Immikkeerteq, Akilertivit and Vittus island. The corundum formation is associated with pegmatite veins in ultramafic rocks. The intrusion of the pegmatite vein into the ultramafic rocks creates different zones, where a cross-section shows a light brown ultramafic rock closer to the pegmatite vein. The ultramafic rock forms a greenish augite/actinolite-rich zone (Fig. 3G, Table S2), followed by a biotite + tschermakite zone towards the centre of the pegmatite intrusion, and can contain corundum, plagioclase, garnet, spinel, kyanite or apatite. The mineral assemblage in the centre of the pegmatitic vein in lherzolite (Fig. 3H) is tschermakite, biotite, corundum, plagioclase, dolomite, hercynite, kyanite, whereas retrograde mineral phases include chlorite, muscovite and calcite. Corundum can locally be up to 5 Vol% of the central zone. The corundum is generally opaque and has a pink to slightly purplish colour. Individual corundum grains are large, up to ~ 5 cm in diameter and up to 10 cm along the c-axis. At Aqqaajaq pegmatite intrusion into dunite creates mineral assemblage of tschermakite, plagioclase, apatite and corundum grains from 4 to 5 mm and up to 5 cm diametre. At Akilertivit the corundum occurs as mm-sized grains in the centre of a black tschermakite layer in the reaction zone. At Tasiilaalik

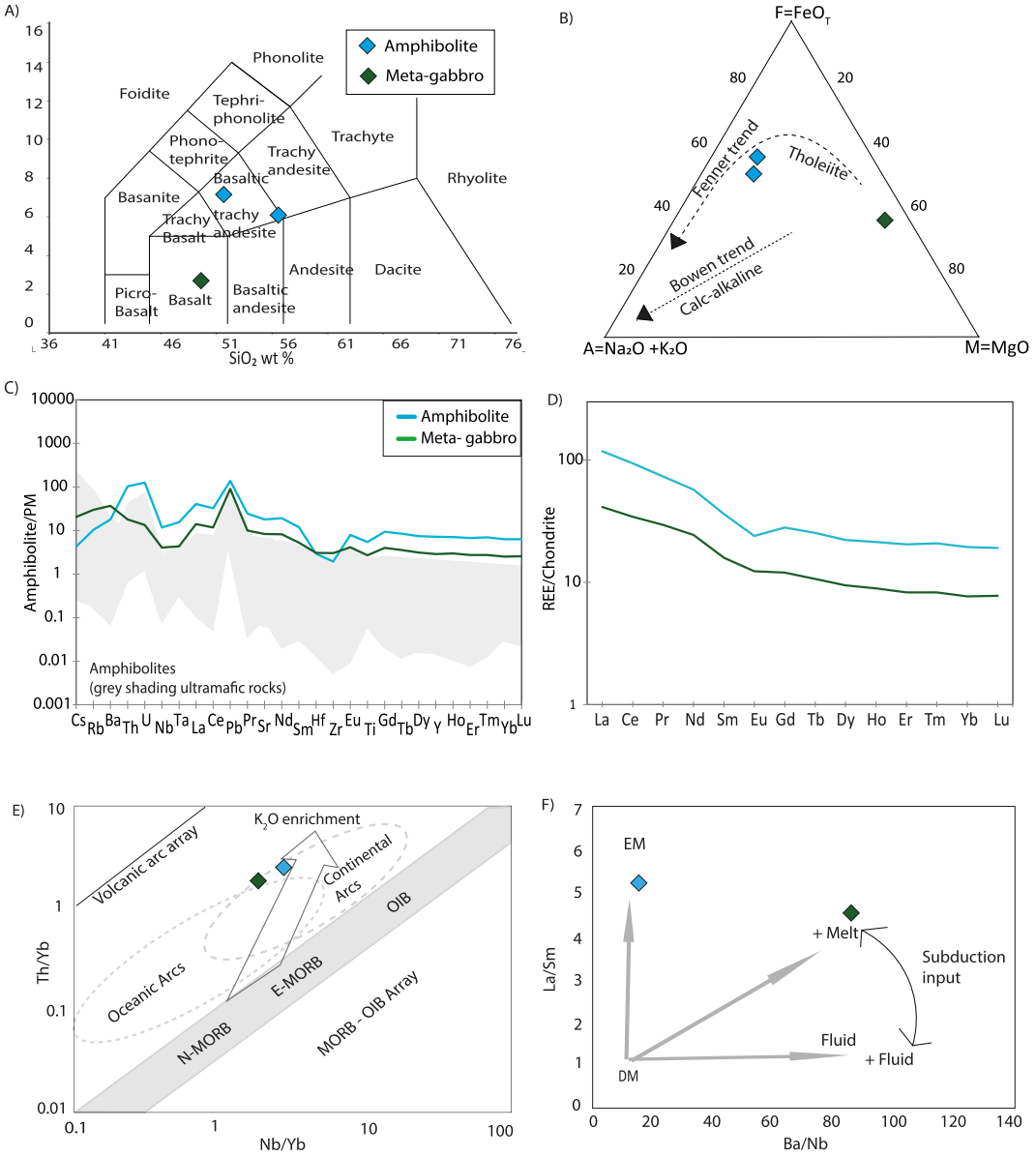

Fig. 5. Two amphibolites from Isertoq and one meta-gabbro. A) In the Total Alkali vs Silica diagram after Le Bas et al. (1986) the amphibolites plot in the basaltic trachy andesite, andesite and basalt field. B) In the AFM discrimination diagram for calc-alkaline and tholeiite igneous rock by Irvine and Baragar (1971) and Vermeesch & Pease (2021), the meta-gabbro plots at the high Mg-end and the two amphibolites plot along the tholeiitic basalt trend. C) Primitive mantle normalized trace elements of the amphibolites. D) Chondrite normalized REE of the amphibolites and ultramafic rocks are enriched compared to dunite. The REE of the amphibolites are enriched in LREE. E) In the Th/Yb vs Nb/Yb diagram modified after Pearce (2008), the amphibolites plot in the E-MORB and the continental arc fields. F) The La/Sm vs Ba/Nb is modified after Langmuir et al. (2006).

(sample 564180, Fig. 4D) the mineral assemblage in lherzolite is coarse blue kyanite, biotite, and microscopic corundum with interstitial plagioclase, as well as retrograde muscovite and chlorite.

4.2. Non-gem quality corundum

The field observations, optical thin section examinations, SEM-EDS and microprobe analyses (Table 3, S2) show that the plumasite-type corundum from the Nattivit area is not ruby or sapphire of gem

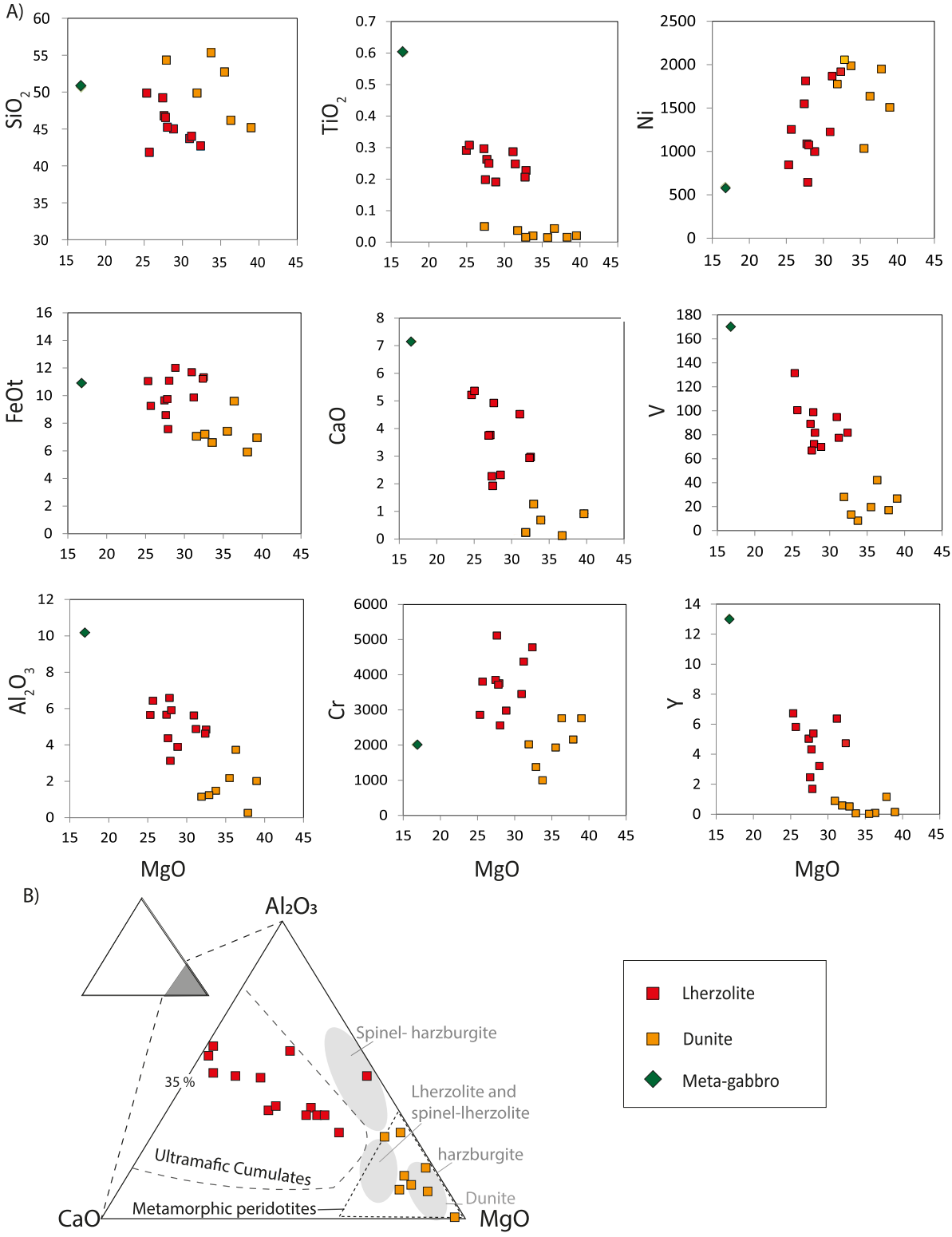

Fig. 6. Harker diagrams (A) of major and trace elements for the ultramafic rocks and the meta-gabbro, and a CaO-Al_2O_3-MgO ternary diagram after Li et al. 2004 (B). The lherzolites from Vittus island, Immikkeerteq, Kitak, Sipportooq and Ajangitap Kangertiva plot away from the dunite from Aqqaajaq, Akilertivit and Tasiilaalik. The lherzolites are more enriched in most elements, except for Mg, Ni and Si. The sample from Qingatak is the meta-gabbro. (For interpretation of the references to colour in this figure legend, the reader is referred to the web version of this article.)

quality, because the grains are translucent to opaque. The plumasite-type corundum hosted in the lherzolite is anhedral. Optical thin section examinations and SEM-EDS analyses indicate that the corundum has a lot of inclusions of rutile, biotite, amphibole and carbonate, and the orientation of the inclusions are random. The corundum on Vittus island and Immikkeerteq (Fig. 3G, 4E-4G) shows massive corundum in the centre of the pegmatite vein in lherzolite. In the plumasite-type corundum hosted in dunite, the grains are generally smaller and anhedral, but some show subhedral to euhedral hexagonal forms (but sample 564130 and 564135 are up to 4 cm). The corundum hosted in the dunite are of non-gem quality due to high amount of fractures and inclusions (Fig. 4H).

The retrogression has not etched or altered the corundum grains (sample 569601), some show a rim, which appears to be minerals that formed during growth of the corundum, rather than retrogressively. The corundum from the Nattivit area is strongly fractured and some show deformation from post-growth effects, where the grains have been sheared and elongated.

4.3. Whole rock geochemistry

4.3.1. Amphibolite and meta-gabbro

There is only whole rock data for two amphibolites and one meta-gabbro (see Table S3 + S4). The rocks have high Na and K contents (Fig. 5A). The amphibolite plot in the basaltic trachy-andesite field, and the meta-gabbro plots in the basaltic field in the Total Alkali Silica diagram after Le Bas et al. (1986) (Fig. 5). In the AFM ($Na_2O + K_2O$-FeO_T-MgO) diagram with AFM boundaries after Vermeesch & Pease (2021) (Fig. 5B), the amphibolites plot in the tholeiitic suite with arc or within-plate affinities, whereas the meta-gabbro plots in the tholeiite MORB field. Primitive mantle normalised values for the incompatible trace elements (Fig. 5C) are high with a positive Pb anomaly and negative Nb + Ta anomalies.

Chondrite normalised REE values show an enrichment in LREE over the HREE (Fig. 5D). There is a slightly negative Eu anomaly, which is interpreted as due to plagioclase fractionation. In the Nb/Yb and Th/Yb diagrams (after Pearce, 2008) (Fig. 5E) the samples are enriched basalts, have K_2O enrichment and plot in the continental arc field. In a Ba/Nb and La/Sm diagram (after Langmuir et al. 2006) (Fig. 5F) the high La/Sm ratio of amphibolite and meta-gabbro of the Isertoq Terrane are shown.

4.3.2. Ultramafic rocks sensu lato

The MgO is between 25.24 and 38.98 wt% and the high Mg content indicates that the rocks are ultramafic (see Fig. 6, Table S3 + S4). The SiO_2 contents range from 40.67 to 46.80 wt%, but a few samples have elevated silica contents of up to 55.35 wt%. The high silica contents indicate modification by metasomatic fluids or plagioclase veining, both of which are observed in the field. In the CaO-Al_2O_3-MgO ternary diagram after Li et al. (2004) two groups of ultramafic rocks are distinguished, where the protoliths are lherzolite and dunite (Fig. 6). The orthopyroxene-rich ultramafic rocks are metamorphosed lherzolite, where the high Ca contents could be due to alteration and addition of Ca. This is seen as a high dolomite content along veins in the rocks. The lherzolite has higher Ti and V than the dunite (Fig. 6), where the difference in Ti content correlates with the presence of accessory ilmenite and chromite in the lherzolite. The large spread in the major elements correlates with changes in the mineral modes of olivine, calcic pyroxene, amphibole and carbonates (Table S2).

The dunites have lower Al contents compared to the lherzolites, and lower Ca and Fe contents (Fig. 6, Table S2 + S3). Mg is higher in the dunites, whereas V, Y and Cr are lower. The Ni content in the dunite samples tends to be higher. Taken together, the ultramafic rocks define a trend that extends to the meta-gabbro from Qingatak. The Th/Sc ratios for all ultramafic rocks are below 1 and Zr/Sc is below 10 (Table S4), which is within the range of compositional variability in magmatic differentiation (after McLennan et al., 1993). The lherzolite is enriched in incompatible elements compared to the dunites, except for Pb (Fig. 7A + 6B). There is significant variability in the most incompatible elements in the lherzolite (Fig. 7A), which could be related to metasomatic overprinting as observed in the field. The Sm/Nd ratios for all ultramafic rocks are between 0.06 and 0.45, but the majority is between 0.24 and 0.21, which is somewhat lower than mantle rocks (0.25–0.29). The lherzolites have higher REE contents, but there is more variability in the dunites (Fig. 7C + 6D). Most samples have a negative Eu anomaly, suggesting plagioclase fractionation at some point in their history. The dunite has a chondrite normalised REE pattern that is flat to U-shaped, whereas the lherzolite shows LREE over HREE enrichment.

The compositions of chromite grains in lherzolite plot at high Cr and Fe + Ti (Fig. 8A) and within the field for zoned intrusions or arc related magmas (after Moreno et al. 2001), but the chromite from the two bands plot in two clusters. They are markedly different from other Archean chromites (Rollinson et al. 2002) from Greenland in the Fiskenæsset complex or Ujarassuit Nunaat from the Nuuk area. In an Al_2O_3 versus TiO_2 diagram (after Kamenetsky et al. 2001) they similarly plot in the arc field, with some overlap to MORB (Fig. 8B).

4.3.3. Schist and calc-silicate rocks

The mica schists and calc-silicate rocks have variable compositions (Table S3) with SiO_2 from 58.65 to 74.45 wt%, Na_2O 1.81–3.35 wt% and K_2O 1.64–4.36 wt%. Al_2O_3 varies from 11.04 to 15.37 wt% and FeO_T 4.62–13.64 wt% (Table 3).

4.4. Rb-Sr, Pb-Pb, Sm-Nd isotopes

4.4.1. Rb-Sr isotopes

The mafic rocks have low $^{87}Rb/^{86}Sr$ and $^{87}Sr/^{86}Sr$ ratios and the lherzolites have the highest $^{87}Sr/^{86}Sr$ ratios (Fig. 9A, Table S5). The sample 569633 plots as an outlier with the highest $^{87}Sr/^{86}Sr$ ratio, which could indicate this sample having been affected by some degree of metasomatic alteration.

4.4.2. Pb isotopes

The dunite samples 569602 and 569603, and meta-gabbro 569624 are the least radiogenic of the samples (Fig. 9B, Table S5). Two linear trends are observed in $^{207}Pb/^{204}Pb$ vs $^{206}Pb/^{204}Pb$ space, one for the dunite and mafic rocks and another for the lherzolite. Initial Pb isotope values are not known, and the errorchron ages were calculated by linear regression following Faure & Mensing (2004), resulting in a model age of 2390 ± 70 Ma for the dunite and mafic rocks, and 2300 ± 380 Ma for the lherzolite. Two groups are present in the $^{208}Pb/^{204}Pb$ vs $^{206}Pb/^{204}Pb$ diagram with Th/U = 5.4 and Th/U = 1.9 (Fig. 9C, Table S5).

4.4.3. Sm–Nd isotopes

The Sm and Nd isotopic compositions are clustered in $^{147}Sm/^{144}Nd$ vs $^{143}Nd/^{144}Nd$ space, except for dunite sample 569602, (Fig. 9D, Table S5). There are also two linear trends, one for the lherzolite and another for the mafic rocks and the dunite. Ages were calculated from slopes with formulas defined by Faure & Mensing (2004), resulting in 2300 ± 270 Ma and 2315 ± 360 Ma for the two trends (Fig. 9D). Both slopes have a high associated uncertainty, but are similar to the ages-calculated from the Pb isotopes. In a plot of initial εNd vs $^{87}Sr/^{86}Sr$, the mafic rocks and dunite fall within the continental crust and continental flood basalt fields, with low εNd and high Sr isotope ratios (Fig. 9E). One dunite sample (569602) has a positive εNd value and a low $^{87}Sr/^{86}Sr$ ratio, and plots near the bulk Earth composition. The lherzolite lie in the field for continental flood basalt and the continental crust. Using the εNd values calculated at 2.3 Ga and plotted vs age (Fig. 9F) reveal depleted mantle curve interceptions (T_{DM} after DePaolo 1981) ranging from 3.4 to 2.8 Ga. Within this range, the mafic rocks have T_{DM} ages of 3.0–2.8 Ga, and the lherzolites and dunite have older T_{DM} ages of 3.4–3.3 Ga. The lherzolite samples 562732, 569611, 569618 are not included in

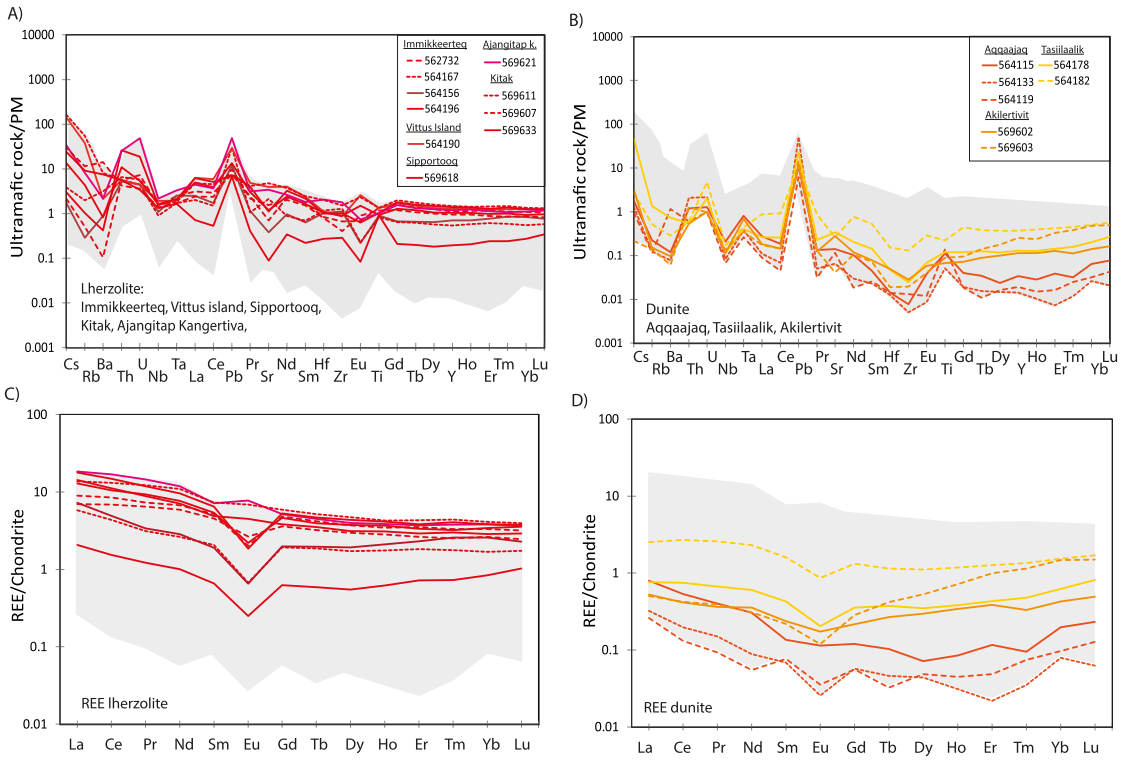

Fig. 7. Multielement plots normalized to Primitive Mantle and REE diagrams normalized to chondrite values after McDonough and Sun (1995). A) Multielement diagram for the lherzolites normalized to Primitive Mantle (PM). There is enrichment in LILE and a peak in Cs, Pb, U and Eu for some samples. Low Nb + Ta, Sr, and Eu are exhibited for some samples. B) The dunites are depleted (ratio below 1) in all elements except Cs, U and Pb. C) Chondrite normalized REE pattern for lherzolites. The grey shading shows all ultramafic rocks. D) Chondrite normalized REE pattern for dunites. The dunites show more variation in the REE pattern compared to the lherzolite.

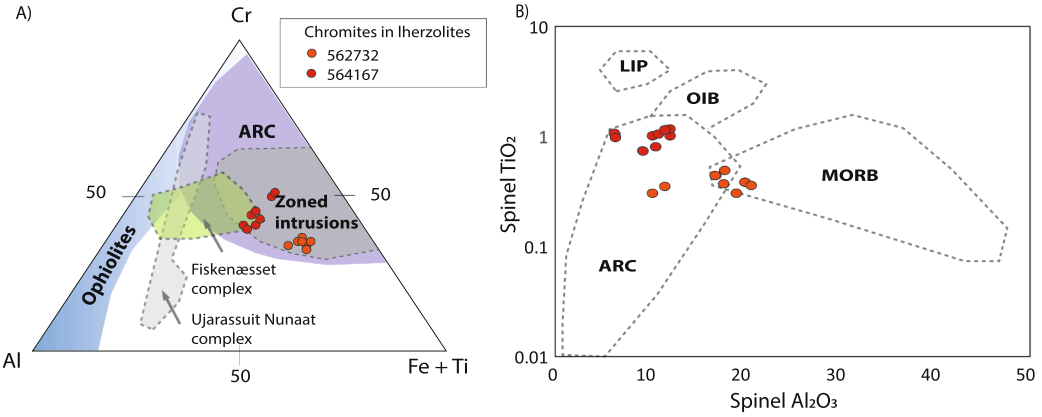

Fig. 8. A) Chromite in lherzolites from the Nattivit area, ternary plot for Al - Cr - Fe + Ti. The samples plot within the field for arc or zoned intrusions. The ophiolite, arc and zoned intrusion fields are after Moreno et al. 2001. Data from Fiskenæsset complex and Ujarassuit Nunaat complex in West Greenland are from Rollinson et al. (2002). B) Al_2O_3 and TiO_2 variation diagram where the two samples plot in the arc field with slight overlap with MORB. The fields for ARC, MORB, OIB and LIP are after Kamenetsky et al. (2001). (For interpretation of the references to colour in this figure legend, the reader is referred to the web version of this article.)

Fig. 9F because of high uncertainty of T_{DM} over 3.7 Ga.

4.5. U-Pb zircon geochronology

Three TTG gneisses, a paragneiss (semi-pelite), a quartzite and five pegmatites were investigated for U-Pb zircon geochronology. Cathodoluminescence and BSE images of the zircons are presented in Fig. 10, the full dataset in Table S6, and the list of age peaks is shown in Table 4. In Fig. 11 all samples are shown graphically in Concordia diagrams and as histograms (90–110 %) $^{207}Pb/^{206}Pb$ ages. The ages are upper $^{207}Pb/^{206}Pb$ intercept ages, where the data-point error ellipses are 2σ. The lower intercept ages are not included, as they could be due to late retrogression in South-East Greenland.

The orthogneisses (564111, 564199, 569625) have magmatic protolith ages between 2860 and 2670 Ma, with metamorphic overprints between 2620 and 2400 Ma and 1885–1850 Ma. The metasedimentary rocks (quartzite and paragneiss) have detrital ages of 2900 to 1930 Ma and metamorphic ages of 1890 ± 9 Ma to 1871 ± 9 Ma, where the latter record the minimum deposition ages for the metasedimentary rocks. Only a few analyses are detrital ages up to 3239 ± 21 Ma. The quartzite

Table 3
Corundum samples from the Nattivit area (see Fig. 2 for localities and Fig. 3-4 for some corundum samples)

Sample No	Locality	Rock type	Metasomatic zone	Crn Colour	Chromophores[a]	Crn size	Minerals
564116	Aqqaajaq	Dunite	Tsr-Crn-Ap	Pink	Cr^{3+}	2–5 mm	Tsr, Crn, Pl, Ru, Ap
564128	Aqqaajaq	Dunite	Tsr-Crn-Ap	Pink	Cr^{3+}	2–5 mm	Bt, Amp, Crn
564130	Aqqaajaq	Dunite	Tsr-Crn-Ap	Pink to purple	Cr^{3+} + Fe^{2+}-Ti^{4+}	4–5 cm	Crn, Pl, Tsr
564135	Aqqaajaq	Dunite	Tsr-Crn-Ap	Pink to purple	Cr^{3+} + Fe^{2+}-Ti^{4+}	1–2 cm	Crn, Pl, Tsr
564180	Tasiilaalik	Lherzolite	Tsr-Crn -Ky	Pink	Cr^{3+}	microscopic	Ky, Crn, Hbl, Bt-Phl, Ba-Fsp, Or, Pl, Zrn, Tsr
564185	Vittus island	Lherzolite	Tsr-Crn-Bt	Pink	Cr^{3+}	up to 10 cm	Crn, Tsr, Bt, Or, Dol, Pl, Zrn, Py, Fc, Act
569601	Akilertivit	Lherzolite	Tsr-Crn-Bt	Pink	Cr^{3+}	2–5 mm	Tsr, Crn, Pl, Ap

[a] Colouring chromophores are afterDubinsky et al. 2020

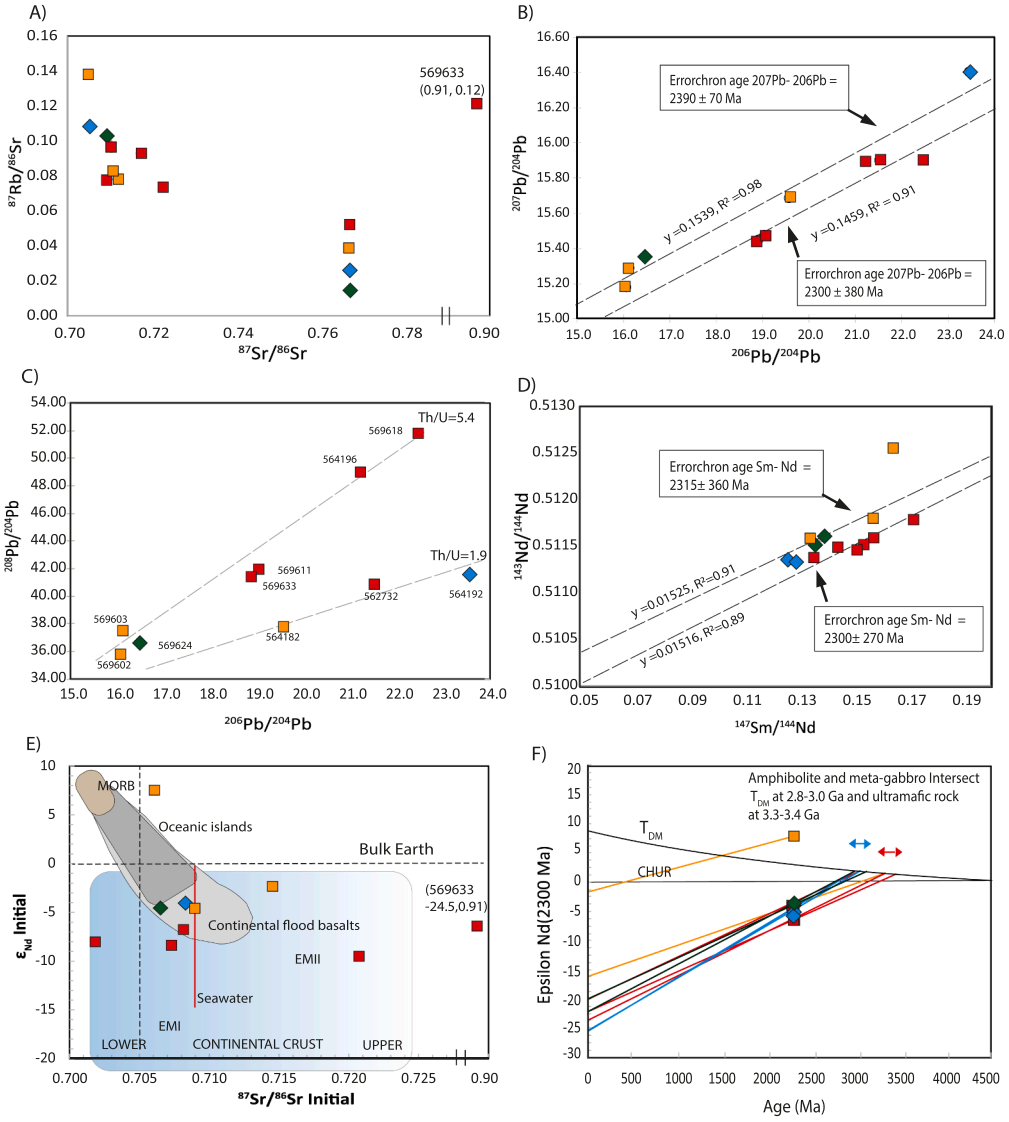

Fig. 9. Sm-Nd, U-Th-Pb and Rb-Sr isotope analyses of the mafic–ultramafic rocks from Nattivit Unit, where the samples are plotted in three groups, amphibolite + meta-gabbro, dunite and lherzolite. A) Rb/Sr vs Sr/Sr plot. B) The meta-gabbro and amphibolite and dunite follow a slightly higher linear trend in the ^{207}Pb-^{206}Pb plot. A model age for ^{207}Pb-^{206}Pb yields 2390 ± 70 Ma for the amphibolites and meta-gabbro, and 2300 ± 380 Ma for the lherzolites. C) ^{208}Pb vs ^{206}Pb show that the lherzolites have a higher Th/U ratio than the other groups. See discussion in the text. D) For the dunites and amphibolites + meta- gabbro, the Sm-Nd model age is 2315 ± 360 Ma, and for the lherzolites the model age is 2300 ± 270 Ma. E) $\varepsilon Nd_{t=2300}$ vs Sr(initial) show that the rocks have similarities to enriched mantle EMI and EMII after Hart (1988) or lower crustal to upper crust. F) An εNd vs age plot indicates that the rocks are derived from an older DM source than indicated by the errorchron age. T_{DM} model age is after Depaulo (1980) and CHUR is Jacobsen & Wasserburg (1984).

(564147) has a higher frequency of Archean ages compared to the paragneiss (564152), which could result from differences in the source. For the three pegmatite generations, the Group 1 pegmatite has U/Pb zircon age peaks at 1873 ± 19 Ma (564143) to 1854 ± 33 Ma (564148). The Group 2 pegmatite has an intrusion age of 1843 ± 4 Ma (564189), where the metasomatized pegmatite (564165) is slightly younger at 1819 ± 14 Ma. The Group 2 pegmatites are related to the corundum formation in the Isertoq Terrane. Age peaks in the Group 1 and 2

Fig. 10. Zircon cathodoluminescense and BSE images of between 3 and 5 chosen characteristic sets of all the zircon grains from each sample. The samples include three TTG gneisses, one paragneiss, one quartzite and five pegmatites.

Table 4
LA-ICP-MSDr zircon U–Pb ages for samples from Isertoq Terrane (see Fig. 2 for localities and Fig. 11 for the main peaks)

Sample	Locality	Rock type	Main age peak	Minor age peaks/range	No. of analyses	Range 90–110 % concondia	bin size
564111	Aqqajaaq	Orthogneiss	1885 ± 11 Ma 2811 ± 17 Ma	2465 ± 47 Ma 2582 ± 22 Ma 2760 ± 13 Ma	111	2870–1810 Ma	25
564199	Tasiilaalik	Orthogneiss	2698 ± 7 Ma 2818 ± 8 Ma	2514 ± 38 Ma 2629 ± 11 Ma	165	2870–1850 Ma	25
569625	Immikkeerteq	Orthogneiss	2623 ± 8 Ma 2667 ± 7 Ma	1857 ± 30 Ma 2527 ± 17 Ma 2789 ± 17 Ma	110	3050–1810 Ma	20
564152	Immikkeerteq	Paragneiss	1871 ± 9 Ma	2735–2345 Ma 2231–2200 Ma	107	2735–1725 Ma	20
564147	Immikkeerteq	Quartzite	1890 ± 9 Ma	2903–2331 Ma 2290–2204 Ma	187	3230–1850 Ma	20
564143	Aqqajaaq	Folded pegmatite (G1)	1873 ± 19 Ma	1794 ± 14 Ma	104	1910–1690 Ma	20
564148	Immikkeerteq	Folded pegmatite (G1)	1854 ± 33 Ma	1780 ± 6 Ma	149	1930–1650 Ma	20
564189	Vittus Island	Pegmatite (corundum-forming) (G2)	1843 ± 4 Ma	older cores in some grains 2885–2100 Ma	141	2810–1730 Ma	20
564165	Immikkeerteq	Pegmatite (corundum-forming) (G2M)	1819 ± 14 Ma	1774 ± 6 Ma	32	1850–1690 Ma	20
569628	Tasiilaalik	Pegmatite (G3)	1754 ± 19 Ma	1833 ± 16 Ma	112	1870–1650 Ma	20

pegmatites around 1774 ± 6 Ma indicate a metamorphic overprint. The Group 3 pegmatite has a peak at 1754 ± 19 Ma (see Fig. 11). See detailed descriptions of the U-Pb zircon analyses in Supplementary file 2. Ages below 1600 Ma in the pegmatites could be related to Pb loss in the zircons, or metamorphic alteration during post-tectonic events in the area.

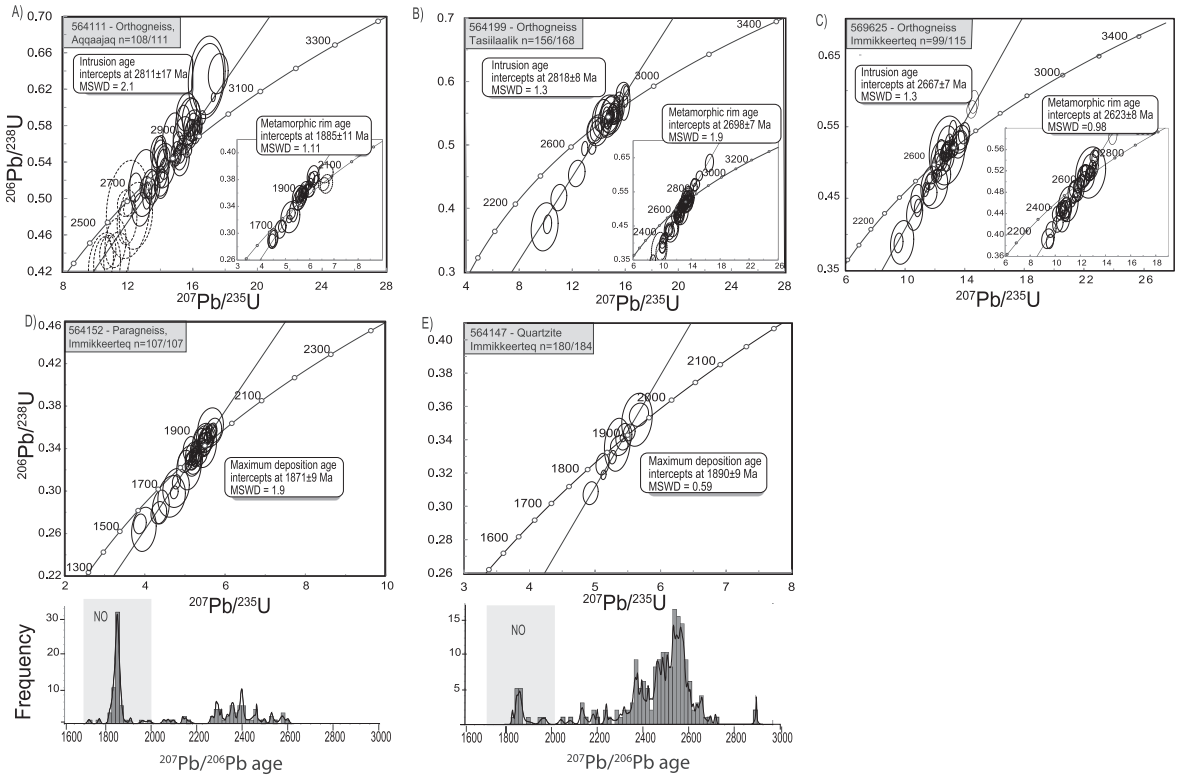

Fig. 11. U-Pb concordia diagrams for U-Pb zircon data (and $^{207}Pb/^{206}Pb$ ages histograms for quartzite and paragneiss). A) TTG gneiss 564111 from Aqqaajaq, B) TTG gneiss 564199 from Tasiilaalik, C) TTG gneiss 569625 from Immikkeerteq. D) Paragneiss 564152 from Immikkeerteq, E) Quartzite 564147 from Immikkeerteq. U-Pb zircon data from the pegmatites F) Group 1 folded pegmatite 564143, G) Group 1 folded pegmatite 564148, H) The corundum-forming pegmatite, Group 2 564189, I) Group 3 pegmatite 569628, J) Desilicified group 2M pegmatite 564165. Isoplot programme 4.15 (Ludwig, 2012) was used for plotting the Concordia-diagrams and AgeDisplay from Thomsen et al. (2016) was used for the $^{206}Pb/^{207}Pb$ histograms. Histograms show $^{207}Pb/^{206}Pb$, 90–110 %. NO = Nagssugtoqidian orogen.

5. Discussion

Here we discuss the geological history of the Isertoq Terrane from the combined dataset of field observations, bulk rock elemental and isotopic compositon and zircon U/Pb age dating, and the implication for corundum formation in relation to the regional crustal development and orogenic processes.

5.1. The (ultra)mafic rocks (Nattivit Unit)

The lherzolite, dunite, amphibolite and meta-gabbro have arc-like affinities in whole rock major and trace elements with elevated Pb and depleted Nb and Ta in chondrite-normalized diagrams, and a tholeiitic trend in the AFM diagram (Fig. 5,6,7). High Fe-Ti in the lherzolite chromites also suggests an arc environment (Fig. 8). Similarly, the rocks fall within a higher continental crust signature in the $\varepsilon Nd_{t=2300Ma}$ vs $^{87}Sr/^{86}Sr$(initial) diagram (Fig. 9). High La/Sm and high Th/Yb at moderate Nb/Yb (Fig. 5) further point to an arc setting with involvement of an enriched mantle component. We suggest that the (ultra)mafic rocks represent remnants which formed in a continental arc environment. However, new age and isotope data presented in this paper for the (ultra)mafic sequence yield Archean ages, and thus these (ultra)mafic rocks are regrouped into the Nattivit Unit.

The lherzolites are more enriched in most elements compared to the dunite, as are the amphibolites compared to the meta-gabbro. The element pattern in the Primitive mantle-normalised multi-element diagrams is however similar, for the lherzolite, and for meta-gabbro and amphibolite. This might indicate that they all are derived from a common source.

The TTG sheets intruded mafic rocks, now represented by amphibolite, an observation in agreement with earlier conclusions by Wager (1934) and Bridgwater et al. (1977). The amphibolite and meta-gabbro in Nattivit Unit give mantle extraction ages of 3.0 to 2.8 Ga from Sm/Nd isotope compositions when plotted in a εNd(2.3 Ga) vs age diagram (Fig. 8F), and the ultramafic rocks give ages of 3.3–3.4 Ga. Although the ultramafic rocks could be derived from an older source, we regard it more likely that these rocks have been disturbed in their isotopic composition by circulating crustal fluids, creating scatter in the T_{DM} model ages. Field relations show that the ultramafic rocks postdate the amphibolite on Immikkeerteq island and were likely sills or dikes rather than cumulates. This means that if they were derived from an older source, this source must have been stored in the crust for an extended period and then largely remobilized, which is difficult to envision for an ultramafic melt. The presence of silicified anthophyllite veins in the ultramafic rocks at Aqqaajaq, and an increase in quantity and size of enstatites in an lherzolite on Vittus island towards the contact with a silicic lithology also indicate interaction with more silicic lithologies or fluids, as does the SiO_2 content up to 57 wt% and the LREE enrichment in the lherzolite. Finally, $^{143}Nd/^{144}Nd$ ratios are low compared to mantle rocks ($^{143}Nd/^{144}Nd > 0.5126$), and the $^{87}Sr/^{86}Sr$ ratios are high with only samples 569603 and 569611 giving bulk-Earth like $^{87}Sr/^{86}Sr$ signatures of around 0.705 (Fig. 8A).

Amphibolite and meta-gabbro have higher Sm, Nd, U, Pb concentrations than the ultramafic rocks, which means that they are more robust to assimilation and metasomatic disturbances to the Sm-Nd and Pb-Pb isotope systems. Indeed, the isotopic signatures in these rocks have less negative epsilon Nd values and unradiogenic Pb compared to the lherzolite. The amphibolite and meta-gabbro rocks show the tightest range in T_{DM} model ages of 3.0 to 2.8 Ga (Fig. 12), and we interpret this as the most reliable estimate for the protolith age for the mafic rocks

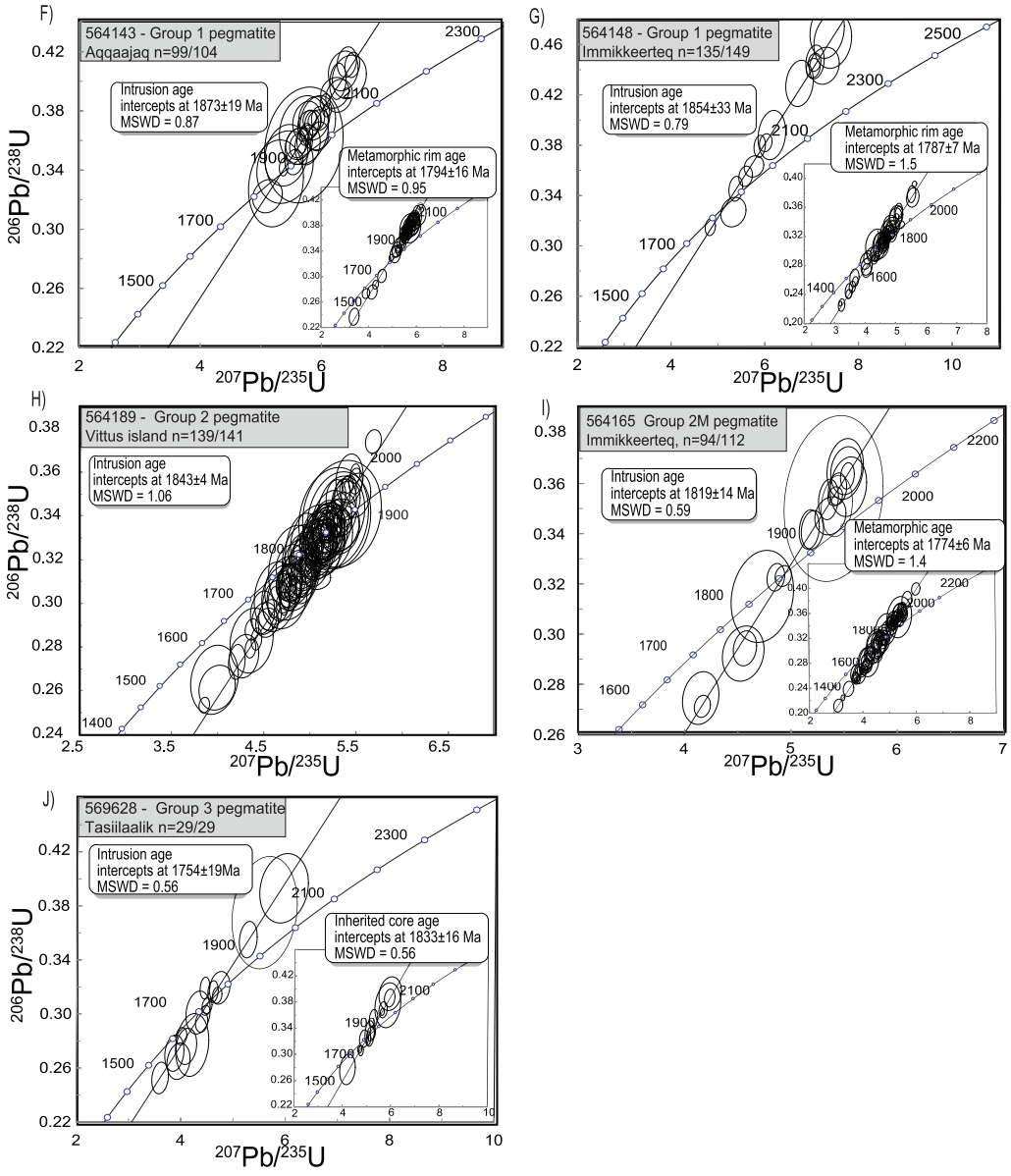

Fig. 11. (*continued*).

(amphibolite and meta-gabbro) in the Nattivit Unit.

The ^{207}Pb-^{206}Pb and Nd-Sm errorchron ages for the (ultra)mafic rock samples are markedly younger at 2.4 to 2.3 Ga (Fig. 9B, 9D). The limited number of samples for the errorchron leads to significant uncertainty in the ages, but all are consistent with the best-constrained age at 2390 ± 70 Ma. The (ultra)mafic rocks were thus affected by an event at this time, following their initial extraction from the mantle in the Archean. There is limited regional data available to indicate what this age may represent. However, dolerite dikes are suggested to intrude the area ~ 2370 Ma (Nilsson et al. 2019) and overlap in age the Scourie Dike Swarm in the Lewisian Gneiss Complex of Scotland (Davies and Heaman, 2014). Other data from the area are εNd and εHf analyses for AIC, which suggests that these magmas were extracted from the mantle between 2500 and 2300 Ma, although only emplaced in the upper crust at ~ 1885 Ma (Lebrun et al. 2018, Kalsbeek & Taylor 1989).

5.2. *The felsic rocks in the Isertoq Terrane*

The TTG gneisses give U-Pb zircon protolith ages of 2818 ± 8 Ma, 2760 ± 13 Ma and 2667 ± 7 Ma, and thus are younger than the 3000–2800 Ma εNd T_{DM} model ages for the (ultra)mafic rocks in the Nattivit Unit (Fig. 12). Presence of ultramafic and amphibolite lenses in the TTG gneiss (e.g., sample 569625), could also indicate that the (ultra) mafic rocks were picked up and included in the TTG sheet at intrusion. There is a marked absence of ages in the TTG gneiss zircon population from 2350 to 2100 Ma, suggesting a period with minimal magmatic and metamorphic activity. The 2350 Ma age peak likely represents the same event recorded in the (ultra)mafic rocks.

Magmatic events occured between 2818 ± 8 Ma to 2667 ± 7 Ma in the Isertoq Terrane based on the U-Pb zircon data and Th/U ratios, where core dates of up to 3044 Ma are interpreted as inherited. The Th/U ratios in the 2800–2650 Ma dates indicate both magmatic and metamorphic events and could be related to activities in South-East Greenland such as the Skjoldungen intrusions (2850–2750 Ma; Kolb

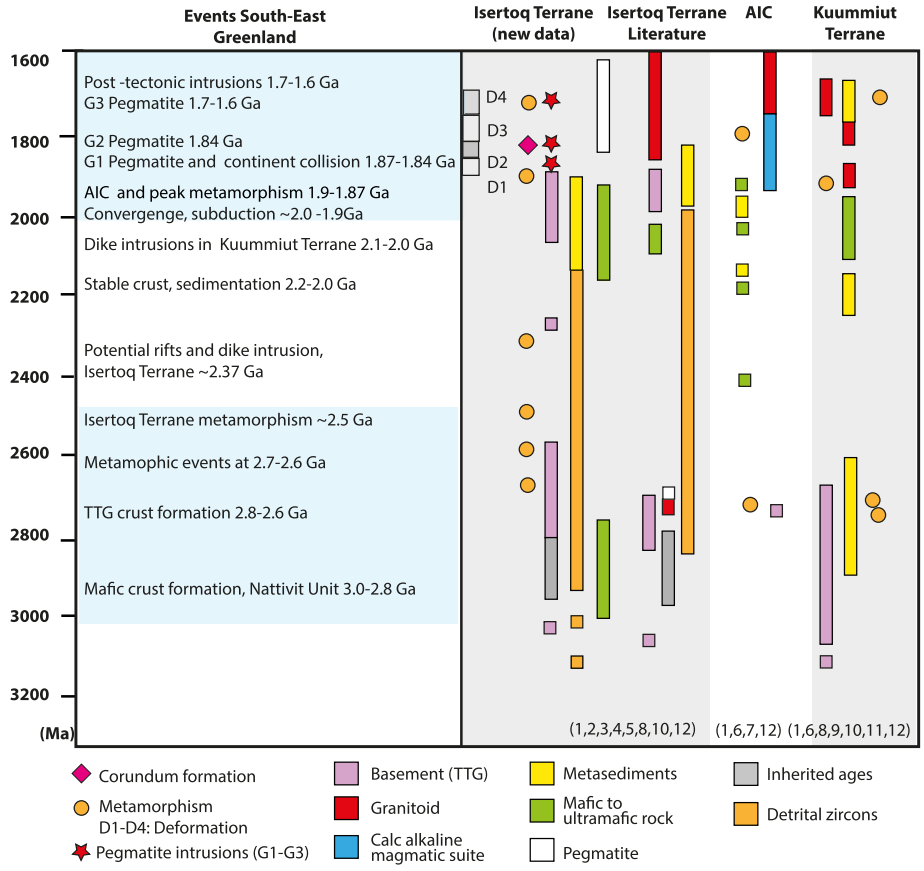

Fig. 12. A compilation of Archean to Palaeoproterzoic events in the NAC and the Nagssugtoqidian Orogen in South-East Greenland. New data are presented for the Isertoq Terrane and literature data from: 1) Kolb et al. 2016, 2) Kolb 2014, 3) Berger et al. 2014, 4) Kalsbeek & Taylor 1989, 5) Nunes et al. 1974, 6) Müller et al. 2018a, b, 7) Lebrun et al. 2018, 8) Nutman et al. 2008, 9) Brooks and Stenstrop, 1989, 10) Kalsbeek et al. 1993, 11) Nicoli et al. 2017, 12) Wright et al. 1973. (For interpretation of the references to colour in this figure legend, the reader is referred to the web version of this article.)

et al. 2013; Kokfelt et al. 2016c), alkaline intrusions (2720–2700 Ma; Berger et al. 2014) and the Singertât Stage (2665 Ma; Bagas et al. 2013). Metamorphic events recorded from zircon rims occur between 2698 ± 7 Ma and 2623 ± 8 Ma and all TTG gneisses record disturbances between 1890 and 1700 Ma (Fig. 11). This is particularly pronounced for TTG gneiss 564111, where the main age peak is at 1885 ± 11 Ma. This age is overlapping with paragneisses recorded in the Isertoq Terrane (Thrane et al. 2016), the timing of intrusion of the Ammassalik Intrusive Complex (Nutman et al. 2008; Lebrun et al. 2018) and the high pressure and temperature stage in the Kuummiut Terrane (Müller et al. 2018b). We interpret the 1885 ± 11 Ma age as the date for peak metamorphism in the Isertoq area.

The zircon dates between 2500 and 2400 Ma could be related to metamorphism (Fig. 12), or due to Pb-loss of another nature. However, the latter is unlikely, as the age group is observed in all three TTG gneisses, and the source area for the metasediments could be the Lewisian gneiss complex of Scotland. The linkage between the Tasiilaq area to the Lewisian gneiss complex are discussed in several papers (Wright et al. 1973; Kalsbeek et al. 1993; Connelly et al. 2000; Friend and Kinny, 2001; Davies & Heaman, 2014), where there are similar rock types, and magmatic and metamorphic events concurrently in both areas.

The Isertoq Terrane marks the northern edge of the North Atlantic Craton, with the adjacent Kuummiut and Schweizerland Terranes belonging to the Rae craton (Fig. 1). In the Kuummiut Terrane, the oldest recorded TTG intrusion age is 3076 ± 14 Ma, while most TTG intrusion ages from Schweizerland and Kuummiut Terrane range from 2795 ± 10 Ma to 2707 ± 15 Ma, with the youngest TTG gneiss at 2646 ± 5 Ma (Kalsbeek et al. 1993; Nutman et al. 2008; Kokfelt et al. 2016a, b, c; Nicoli et al. 2017). It is uncertain how far apart the Isertoq and Kuummiut Terrane were in Archean time, but since they represent separate terranes, it is unlikely that the two terranes experienced the same geological history and crustal development (Fig. 12).

5.3. *Metasedimentary rocks in the Kap Tycho Brahe Unit*

There was an oblique subduction of the Kuummiut Terrane below Isertoq Terrane during the Nagssugtoqidian Orogeny, which caused an imbricated SE-vergent thrust and ramp system. The meta-sedimentary units (quartzite, paragneiss, mica schist) are Paleoproterozoic and in direct contact to the Archean mafic to ultramafic rocks in the Isertoq Terrane. An example of this is observed at northern end of Immikkeerteq island, where there is an age break (unconformity) between the TTG gneiss and the quartzite + mica schist, and an age gap between the Paleoproterozoic paragneiss in direct contact to the Archean amphibolites on Immikkeerteq (Fig. 3A). These field relationships are supported by the zircon ages. The quartzite from Immikkeerteq records a range in U-Pb zircon ages from 3230 to 1850 Ma. The Archean age peaks in the quartzite overlap, at least in part, with the felsic TTG gneisses in the Isertoq Terrane. The main peak is at 1890 ± 9 Ma, which is contemporaneous to the peak metamorphism and is the minimum deposition age for the quartzite. The date agrees with a paragneiss collected at Tasiilaalik with a peak between 2050 and 1900 Ma (Thrane et al. 2016). This age is also consistent with ages reported by Nutman et al. (2008) in a kyanite schists from the Kuummiut Terrane. Interestingly, age peaks are present in meta-sedimentary rocks in the 2350 to 2100 age gap of the TTG gneiss, at 2270 Ma and 2210 Ma, which indicate an additional source of material other than the Isertoq Terrane. Zircons in the paragneiss range in age from 2735 to 1725 Ma, and the main peak at 1871 ± 9 Ma, which is interpreted as the minimum desposition age. The different age range and the Th/U ratios in the quartzite and paragneiss could indicate two slightly different sources for the detrital zircons.

5.4. Nagssugtoqidian Orogen

The (ultra)mafic and TTG rocks make up the basement of the Isertoq Terrane and are of Archean to earliest Proterozoic age, where only the meta-sedimentary rocks, the pegmatites and syn-tectonic-to post-tectonic intrusions are younger. The oldest recorded peaks in the U-Pb zircon data related to the Nagssugtoqidian Orogeny occur at 1890 ± 9 Ma to 1871 ± 9 Ma, which we interpret to peak metamorphism in Isertoq Terrane. These estimates are largely consistent with the data from Nutman & Friend (1989) for high-pressure granulite meta-dolorite from Kitak, which was metamorphosed at 650–660 °C and 7–8.5 kbar. The TTG gneisses in the Isertoq Terrane record a metamorphic age peak at 1885 ± 11 Ma, which is similar to intrusion ages of the AIC (Lebrun et al. 2018) for granodiorite at 1911 ± 7 Ma, anorthosite veins at 1887 ± 8 Ma and gabbronorites at 1882 ± 9 Ma. Overall, magmatic activity of the AIC is suggested to have occurred between 1910 and 1870 Ma (Lebrun et al. 2018) and is interpreted to represent a continental magmatic arc (Kalsbeek & Taylor, 1989; Nutman et al. 2008) or was formed by assimilation of partial melts of the garnetfereous host rock (Lebrun et al. 2018). Likewise, Nutman et al. (2008) notice a great similarity in the timing of metamorphism between Kuummiut and Isertoq terranes (Fig. 12).

The pegmatites record ages that correspond to convergence and deformation during the Nagssugtoqidian Orogeny (Figs. 11, 12). The pegmatites post-date the peak metamorphic stage. The Group 1 pegmatites have a concordia protolith intercept age of 1873 ± 19 Ma based on U-Pb zircon geochronology and a metamorphic rim age of 1794 ± 14 Ma. During fieldwork it was observed that Group 1 pegmatites are folded, quartz-rich and not associated with corundum. The Group 2 pegmatite have a concordia intercept age at 1843 ± 4 Ma which is interpreted as the intrusion age. Intrusion of the Group 2 pegmatites triggered corundum formation. Group 2M pegmatite have a concordia intercept age of 1819 ± 14 Ma and a metamorphic rim at 1774 ± 6 Ma. The 1819 ± 14 Ma age is interpreted as the magmatic intrusion age. The post-tectonic Group 3 pegmatite crosscut Group 2 pegmatites, and we interpret their U-Pb zircon ages to reflect intrusion at 1754 ± 19 Ma.

5.5. Implications for corundum formation

Corundum occurrences are remarkably common in the Isertoq Terrane and all occur where Group 2 (including 2 M) pegmatites interact with ultramafic rocks, but they appear absent in the rest of the Tasiilaq area. Pegmatite sheets are observed throughout the Tasiilaq area, in all terranes, and include several generations. Ages for the pegmatites in Kuummiut Terrane are 1858 ± 7 Ma and 1663 ± 9 Ma (Thrane et al. 2016), which overlap with Group 1 and 3 pegmatites, respectively. However, no pegmatite ages overlapping with the group 2 pegmatites have been found from the Kuummiut Terrane.

The field observations indicated a desilification process of the pegmatite at progressive reaction with the ultramafic rocks, which produced a metasomatic reaction zone with a symmetric zonation parallel to the pegmatite vein. The resulting metasomatism progressively desilicifies the pegmatite, decreases its quartz and feldspar contents and culminates in a layer of biotite with a centre of tschermakite and corundum. This reaction progression can be traced in-situ from the point where the pegmatite intruded into the ultramafic rock, and corundum formation can therefore be conclusively dated contemporaneous with pegmatite intrusion. The different groups of pegmatites all have a metasomatic reaction rim with ultramafic rocks, for example the formation of sillimanite segregations adjacent to pegmatites in the Helheim Unit metapelites or a metasomatic reaction between an ultramafic rock and a pegmatite is described in Hinsberg & Poulsen (2017) from the Kuummiut Terrane, however no corundum is observed. No geochemical data on the pegmatite composition of the Kuummiut Terrane is available for comparison. However, only the Group 2 + 2M was corundum forming, which indicates that the geochemical composition of the pegmatite melt/fluid is important. The reaction products of the different generations of pegmatites and ultramafic rocks are not the same, which is observed at Sipportooq and Kitak where Group 3 pegmatite reacted with the ultramafic rocks forming apatite and ilmenite, but no corundum.

Corundum is formed in both the metamorphic lherzolite and the dunite, which indicates the role of the ultramafic rocks as a silica sink as an important factor, and that the type of ultramafic rock is not the determining factor for corundum formation. Ultramafic lithologies including Archean dunites and spinel harzburgites are reported Peters et al. (2020) from the Kuummiut Terrane, hence the lack of corundum can therefore not be attributed to the absence of ultramafic rocks in other terranes.

Most plumasite-type corundums have non-gem quality with only a few places having *gem* quality ruby/sapphire such as Kashmir (India) and Umba (Tanzania) (Guiliani et al. 2020) (Table 5). The potential gem factors that affect the growth of a crystal and the gemstone quality, include the type of nucleation (small or large crystals), fast/rough or slow/smooth growth, time required for growth, limited and desired amounts of inclusions, good stability during growth, free space available or within a rock in competition with other minerals, and lastly the syn- to post-growth effects such as retrogression, deformation, ecthing or fracturing (Fritsch et al. 2017). The plumasite-type corundum in the lherzolite and dunite was competing with the space available with other minerals forming at the same time, where the inclusions show random orientation, which indicates fast or rough growth, and therefore the corundum did not create clear crystals during growth. The corundum formed in the most evolved part of the pegmatite fluid/melt and along with biotite and tschermakite in the metasomatic reaction zone in lherzolite, where biotite and tschermakite inclusions indicate that the corundum formed last. The fractures in the corundum are likely caused by decompression during uplift and orogenic collapse. Corundum in the lherzolite is massive and in the dunite the grains are more sporadic, which could indicate some differences in either a) space available during growth, b) differences in the geochemical evolution and the pegmatite during metasomatism, the amount of fluids available in the corundum forming part of the metasomatic reaction zone, the element mobility and speciation in the fluids.

The Isertoq Terrane was the upper plate during convergence and the corundum forming pegmatites from Group 2 appear to be restricted to the Isertoq Terrane both in time and in location. This could imply that the geotectonic setting is important for generating plumasite-type corundum and the melt/fluids could be derived from either anatectic melt of the lower crust, or partial melt of the subducted continental crust, or metasomatic fluids from the subducted plate released into the mantle wedge. The composition of the ultramafic rocks during metasomatism only seem to play a minor role, if at all.

According to Stern et al. (2013) metamorphic ruby and sapphire are petrogenetic indicators and products of continent collision as corundum formation occurs at amphibolite to granulite facies conditions in the upper plate of collisional metamorphic terranes. When comparing their model for continent collision, the emplacement of the AIC could fit into the collisional metamorphic terranes, but the plumasite-type corundum (this study) are formed in the overriding plate in the (ultra)mafic suites in Nattivit Unit, in the continental crust.

A key observation of corundum formation in the Isertoq Terrane is that it forms a regular and predicticable part of the geological history of the area. The presence of ultramafic lithologies in the mafic rock (amphibolite and meta-gabbro) and TTG gneiss, and the intrusion of pegmatite with a specific geochemical composition made their interaction a near certainty, and corundum is the outcome of the style of metasomatism that ensues.

6. Conclusion

The new data from the Isertoq Terrane reveal the crustal

Table 5
Plumasite-type corundum.

Locality[a]	Country	Minerals	Host rock	Temperature	Pressure	References
Plumas	California	Pl ± Crn ± Ms ± Mrg	Peridotite			Lawson 1903
Corundum Hill mine	North Carolina	Crn ± Chl ± Spl	Dunite	750–800	8–9 kbar	Pratt 1901
Mangare	Kenya	Crn ± An ± Ms ± Zo	Serpentinite	500 °C	5 kbar	Simonet 2000; Mercier et al. 1999; Key & Ochieng, 1991
Umba	Tanzania		Serpentinite			Seifert & Hyrsl, 1999
Polar Urals	Russia	Pl ± Phl ± Crn ± Chr	Dunite + harzburgite	600–700 °C	10–11 kbar	Ishimaru et al. 2015; Vakhrusheva & Ivanov 2018; Meng et al. 2018
South Urals	Russia	Crn ± Sp ± Chl ± Ms	Orthopyroxenites	700–750 °C	1.8–3.5 kbar	Sorokina et al. 2019
Sumjam deposit	India	Crn ± Pl ± Tur ± Ms	Amphibolite	680–700 °C	3.7–5.6 kbar	La Touche 1890; Atkinson and Kothavala, 1983
Allier Valley	France	Pl ± Pl ± Crn ± Sp ± Bt ± Zrn ± Urn	Harzburgite			Forestier & Lasnier, 1969
Naxos	Greece	Crn ± Phl ± Tur	Clinopyroxenite	580–750 °C	4–7 kbar	Voudouris et al. 2019
O'Briens Claims	Zimbabwe	Crn ± Chl ± Cr-Ms	Komatiite	400–500 °C	5.5–7.4 kbar	Kerrick et al., 1987; Schreyer, 1988
Limpopo	South Africa	Crn ± Fsp ± Ms	Amphibolite			Robb & Robb, 1986
Nattivit	Greenland	Crn ± Pl ± Bt ± Tsr	Lherzolite + dunite	530–800 °C	4.2–10 kbar	This study

[a] see Guiliani et al. 2020 for details on the different localities, and mineral abbreviations after Warr 2021.

development prior to Nagssugtoqidian deformation and continent collision. The Archean rocks in the Isertoq Terrane consist of (ultra) mafic rocks and TTG gneiss. The mafic rocks have 3000–2800 Ma T_{DM} model ages, with 2820–2670 Ma U-Pb zircon ages for the TTG gneisses. The field observations indicate that the metamorphic dunite and lherzolite are intrusive into the amphibolites, before the TTG sheets intruded the amphibolite. The geochemical signatures in the (ultra)mafic rocks indicate they are formed in a continental arc setting. Metamorphic events occurred at 2698 ± 7 Ma to 2629 ± 11 Ma, 2500–2400 Ma and1900–1600 Ma. A metasomatic event occurred around ~ 2370, possibly from a continental rifting event and intrusion of a mafic dike swarm, where circulating crustal fluids partly reset the isotopic signature in the (ultra)mafic rocks in the Nattivit Unit. A break in ages around 2350–1900 Ma in the TTG gneisses is interpreted as a period with a minimal magmatic/metamorphic activity.

The Nagssugtoqidian Orogeny started ~ 2000 Ma when the Rae Craton and NAC started to converge Peak metamorphism occurred between 1890 ± 9 to 1871 ± 9 Ma with the metamorphic mineral assemblages indicating pressure and temperatures of upper amphibolite facies conditions in the Isertoq Terrane. The Group 1 to 3 pegmatite intrusion occurs between 1873 ± 19 and 1754 ± 19 Ma, where the corundum forming Group 2 pegmatite have a U-Pb zircon age of 1843 ± 4 Ma. Both lherzolite and dunite can host plumasite-type corundum, and corundum formation is triggered by metasomatic reaction of pegmatites and ultramafic rock, in a magmatic arc geotectonic setting.

Credit authorship contribution statement

Majken D. Poulsen: Writing – original draft, Conceptualization, Formal analysis, Visualization, Investigation, Funding acquisition. **Nynke Keulen:** Supervision, Project administration, Conceptualization, Writing – review & editing. **Vincent J. van Hinsberg:** Methodology, Pseudosection modelling, Review & Editing. **Jochen Kolb:** Supervision, Writing – review & editing. **Robert Frei:** Radiogenic isotope analysis. **Tonny B. Thomsen:** LAICPMS zircon U/Pb zircon dating.

Declaration of Competing Interest

The authors declare that they have no known competing financial interests or personal relationships that could have appeared to influence the work reported in this paper.

Data availability

I have shared the link to my data/at the attached File step

Acknowledgments

This work is part of a PhD project and was supported by the Danish State Fund for Arctic Research and the Geological Survey of Denmark and Greenland (80.15). The authors would like to thank the following people from GEUS: Mojagan Alaei for help with zircon preparation for LA-ICP-MS U-Pb zircon dating, Olga Nielsen for preparation and analysis for major and trace elements, Toke Hvenegaard for sample preparation for geochemical analysis and thin section preparation and Simon Hansen Serre and Maja B. Rasmussen for help with set up to LA-ICP-MS analysis. Thomas F. Kokfelt is thanked for discussion on U-Pb zircon data interpretations and the geology of South-East Greenland. Christina N. Jensen from Department of Geosciences and Natural Resource Management at Copenhagen University is thanked for help with ion chromotographic procedures and preparation for TIMS analysis. We would like to thank Scott Boroughs from the Peter Hooper GeoAnalytical Lab in Washington State University for major element analyses for ultramafic rocks. We would like to thank Vittus Sakæussen, the 2009-winner of the Greenlandic national mineral hunt for guiding us to his corundum locality in 2014. We also thank Dan & Marie Reimer and Hans Christian Florian for boat assistance during field work in the Tasiilaq area in 2014 and 2015.

Appendix A. Supplementary material

Supplementary data to this article can be found online at https://doi.org/10.1016/j.precamres.2022.106940.

References

Andrews, J.R., Bridgwater, D., Gormsen, K., Gulson, B., Keto, L., Watterson, J., 1973. The Precambrian of South-East Greenland. In: Park, R.G., Tarney, J. (Eds.), The Precambrian of Scotland and Related Rocks of Greenland. U.P. Birmingham, Birmingham, pp. 143–156.
Atkinson, D., Kothavala, R.Z., 1983. Kashmir sapphire. Gems Gemol. 19, 64–76.
Bagas, L., Næraa, T., Kolb, J., Reno, B.L., Fiorentini, M.L., 2013. Partial melting of theArchaean Thrym Complex of southeastern Greenland. Lithos 160–161, 164–182.
Berger, A., Kokfelt, T., Kolb, J., 2014. Exhumation rates in the Archaean from pressure-time paths: example from the Skjoldungen Orogen. Precambr. Res. 255, 774–790.
Bridgwater, D., 1976. Nagssugtoqidian mobile belt in East Greenland. In: Escher, A., Watt, W.S. (Eds.), Geology of Greenland. The Geological Survey of Greenland, Copenhagen, pp. 97–103.

Bridgwater, D., Gormsen, K., 1968. Precambrian rocks of the Angmagssalik area, East Greenland. Rapp. Grønlands geologiske Undersøgelse 15, 61–71.
Bridgwater, D., Davies, F.B., Gill, R.C., 0, Gorman, B. E., Henriksen, N. & Watterson, J., 1977. Field mapping in the Nagssugtoqidian of South-East Greenland. Rapp. Grønlands geol. Unders. 85, 74–83.
Bridgwater, D., Austrheim, H., Hansen, B.T., Mengel, F., Pedersen, S., Winter, J., 1990. The Proterozoic Nagssugtoqidian mobile belt of southeast Greenland: A link between the eastern Canadian and Baltic shields. Geosci. Can. 17 (4), 305–310.
Brooks, C.K., Stenstrop, G., 1989. The Ivnartivaq complex, Sermilik, Ammassalik. In: Kalsbeek, F. (ed.), Geology of the Ammassalik Region, South-East Greenland. Grønlands Geologiske Undersøgelse (GGU), Rapport 146, Copenhagen, 87-91.
Chadwick, B., Dawes, P.R., Escher, J.C., Friend, C.R.L., Hall, R.P., Kalsbeek, F., Nielsen, T.F.D., Nutman, A.P., Soper, N.J., Vasudev, V.N., 1989. The proterozoic mobile belt in the Ammassalik region, South-East Greenland (Ammassalik mobile belt): an introduction and re-appraisal. In: Kalsbeek, F. (ed.), Geology of the Ammassalik region, South-East Greenland. Grønlands Geologiske Undersøgelse, Rapport 146, 5-16.
Chadwick, B., Vasudev, V.N., 1989. Some observations on the structure of the Early Proterozoic, Ammassalik mobile belt in the Ammassalik region, South-East Greenland. In Geology of the Ammassalik region, South-East Greenland. Grønlands Geologiske Undersøgelse, Rapport 146, 29–41.
Connelly, J.N., Gool, J.A.M., Mengel, F.C., 2000. Temporal evolution of a deeply eroded orogen: the Nagssugtoqidian Orogen, West Greenland. Can. J. Earth Sci. 37, 1121–1142.
Davies, J.H.F.L., Heaman, L.M., 2014. New U-Pb baddeleyite and zircon ages for the Scourie dyke swarm: A long-lived large igneous province with implications for the Paleoproterozoic evolution of NW Scotland. Precambr. Res. 249 (2014), 180–198.
Dawes, P.R., Soper, N.J., Escher, J.C., Hall, R.P., 1989. The northern boundary of the Proterozoic (Nagssugtoqidian) mobile belt of South-East Greenland. In: Kalsbeek, F. (ed.), Geology of the Ammassalik Region, South-East Greenland. Grønlands Geologiske Undersøgelse, Rapport 146, 54-65.
DePaolo, D.J., 1981. Neodymium isotopes in the Colorado Front Range and crust – mantle evolution in the Proterozoic. Nature 291, 193–197.
Dubinsky, E.V., Stone-Sundberg, J., Emmett, L.M., 2020. A Quantitative Description of the Causes of Color in Corundum. Gems & Gemology, Spring 2020, Vol. 56, No. 1, 2-28.
Escher, J.C., Friend, C.R.L., Hall, R.P., 1989. The southern boundary zone of the Proterozoic mobile belt, South-East Greenland: geology of the region between Gyldenløve Fjord and Isertoq. In: Kalsbeek, F. (ed.), Geology of the Ammassalik Region, South-East Greenland. Grønlands Geologiske Undersøgelse, Rapport 146, 70-78.
Escher, J.C., 1990. 1:500.000 Geological Map of Greenland: Sheet 14, Skjoldungen. Geological Survey of Denmark and Greenland, Copenhagen.
Faure, G., Mensing, T.M., 2004. Isotopes: Principles and Applications. Wiley, 3nd Edition, 928 pp.
Feenstra, A., 1985. Metamorphism of Bauxites on Naxos, Greece. Ph.D. dissertation. In: Geologica Ultraiectina, 39. Utrecht University, p. 206–pp.
Forestier, F., Lasnier, B., 1969. Découverte de niveaux d'amphibolites à pargasite, anorthite, corindon et sapphirine dans les schistes cristallins du Haut-Allier. Contrib. Mineral. Petrol. 23, 194–235.
Frei, R., Polat, A., 2013. Chromium isotope fractionation during oxidative weathering – implications from the study of a Paleoproterozoic (ca. 1.9 Ga) paleosol, Schreiber Beach. Ontario. Can. Precambr. Res. 224, 434–453.
Friedman, E., Polat, A., Thorkelson, D.J., Frei, R., 2016. Lithospheric mantle xenoliths sampled by melts from upwelling asthenosphere: the Quaternary Tasse alkaline basalts of southeastern British Columbia, Canada. Gondwana Res. 33, 200–230.
Friend, C.R.L., Kinny, P.D., 2001. A reappraisal of the Lewisian Gneiss Complex: geochronological evidence for its tectonic assembly from disparate terranes in the Proterozoic. Contribution to Mineralogy and Petrology Jan. 2001, Vol. 142,198-218.
Fritsch, E., Rondeau, B., Devouard, B., Pinsault, L., C.,, 2017. Why are some crystals gem quality? Crystal growth considerations on the "gem factor". Can. Mineral. 55, 521–533. https://doi.org/10.3749/canmin.1700013.
Garde, A.A., Hollis, J.A., 2010. A buried Palaeoproterozoic spreading ridge in the northern Nagssugtoqidian orogen, West Greenland. Geol. Soc. Lond. Spec. Publ. 338 (1), 213–234.
Garde, A.A., Marker, M., 1988. Corundum crystals with blue-red colour zoning near Kangerdluarssuk, Sukkertoppen district, West Greenland. Rapp. Grønl. Geol. Unders. 140, 46–49.
Garnier, V., Giuliani, G., Ohnenstetter, D., Fallick, A.E., Dubessy, J., Banks, D., et al., 2008. Marble-hosted ruby deposits from Central and Southeast Asia: Towards a new genetic model Ore Geol. Rev. 34 (1–2), 169–191.
Giuliani, G., Ohnenstetter, D., Fallick, A.E., Groat, L., Fagan, A.J., 2014. Chapter 2: The Geology and genesis of gem corundum deposits. Mineralogical Association of Canada Short Course 44, Tucson AZ, February 2014, 29-112.
Giuliani, G., Groat, L.A., Fallick, A.E., Pignatelli, I., Pardieu, V., 2020. Ruby Deposits: a review and geological classification. Minerals 2020, 10, 597; doi:10.3390/min10070597, 83 pp.
Hall, R.P., Chadwick, B., Escher, J.C., Vasudev, V.N., 1989a. Supracrustal rocks in the Ammassalik region, South-East Greenland. In: Kalsbeek, F. (ed.), Geology of the Ammassalik Region, South-East Greenland. Grønlands Geologiske Undersøgelse (GGU), Rapport 146, Copenhagen, 17-22.
Hall, R.P., Hughes, D.J., Joyner, L., 1989b. Basic dykes of the southern Ammassalik region, South-East Greenland: preliminary mineralogical and geochemical results. In: Kalsbeek, F. (ed.), Geology of the Ammassalik Region, South-East Greenland. Grønlands Geologiske Undersøgelse (GGU), Rapport 146, Copenhagen, 79-82.
Hart, S.R., 1988. Heterogeneous mantle domains: signatures, genesis and mixing chronologies. Earth Planet. Sci. Lett. 90, 273–296.
Hellstrom, J., Paton, C., Woodhead, J., Hergt, J., 2008. Iolite: Software for spatially resolved LA- (quad and MC) ICPMS analysis. In: Sylvester, P. (Ed.), Laser Ablation ICP–MS in the Earth Sciences: Current Practices and Outstanding Issues, Mineral. Assoc. of Canada, Quebec, Canada, pp. 343–348.
Hinsberg, V.J.V., Poulsen, M.D., 2017. 2014 Field report - investigations of the metamorphic rocks in the Tasiilaq area, South-East Greenland (SEGMENT-project). Danmarks og Grønlands Geologiske Undersøgelse, rapport 2017/42., 129 pp.
Hinsberg, V.J.V., Yakymchuk, C., Jepsen, A.T.K., Kirkland, C.L., Szilas, K., 2021. The corundum conundrum: Contraining the compositions of fluids involved in corundum formation. Chem. Geol. 20 June, 120180 https://doi.org/10.1016/j.chemgeo.2021.120180.
Horwitz, E.P., Chiarizia, R., Dietz, M.L., 1992. A novel strontium-selective extraction chromatographic resin. Solvent Extract. Ion Exchange 10, 313–336.
Irvine, T.N., Baragar, W.R.A., 1971. A guide to the chemical classification of the common volcanic rocks. Can. J. Earth Sci. 8, 523–548. https://doi.org/10.1139/e71-055.
Ishimaru, S., Arai, S., Miura, M., Shmelev, V., Pushkarev, E., 2015. Ruby-bearing feldspathic dyke in peridotite from Ray-Iz ophiolite, the Polar Urals: Implications for mantle metasomatism and origin of ruby. J. Mineral. Petrol. Sci. 110, 76–81.
Jackson, S.E., Pearson, N.J., Griffin, W.L., Belousova, E.A., 2004. The application of laser ablation-inductively coupled plasma-mass spectrometry to in situ U-Pb zircon geochronology. Chem. Geol. 211, 47–69.
Jacobsen S.B., Wasserburg G.J., 1984. Sm-Nd isotopic evolution of chondrites and achondrites, II. Earth and Planet. Sci. Lett. 1984. Vol. 67, 137-150.
Kalsbeek, F., Taylor, P.N., 1989. Programme of geochronology and isotope geochemistry in the Ammassalik region, South-East Greenland: outline and preliminary results. In The geology of the Ammassalik region, South-East Greenland. Grønlands Geologiske Undersøgelse Rapport 146, 13–16.
Kalsbeek, F., Austrheim, H., Bridgwater, D., Hansen, B.T., Pedersen, S., Taylor, P.N., 1993. Geochronlogy of Archean and Proterozoic events in the Ammassalik area, South-East Greenland, and comparisons with the Lewisian of Scotland and the Nagssugtoqidian of West Greenland. Precambr. Res. 62, 239–270.
Kalsbeek, F., (ed.), 1989. The geology of the Ammassalik region, South-East Greenland. Grønlands Geologiske Undersøgelse (GGU) Rapport 146, 105 pp.
Kamenetsky, V.S., Crawford, A.J., Meffre, S., 2001. Factors controlling chemistry of magmatic spinel: an empirical study of associated olivine, Cr-spinel and melt inclusions from primitive rocks. J. Petrol. 42, 655–671.
Kerrick, R., Fyfe, W.S., Barnett, R.L., Blair, B.B., Willmore, L.M., 1987. Corundum, Cr-muscovite rocks at O'Briens, Zimbabwe: the conjunction of hydrothermal desilicification and LIL-element enrichment – geochemical and isotopic evidence. Contrib. Mineral. Petrol. 95, 481–498.
Keulen, N., Schumacher, J.C., Næraa, T., Kokfelt, T.F., Scherstén, A., Szilas, K., van Hinsberg, V.J., Schlatter, D.M., Windley, D., 2014. Meso- and Neoarchaean geological history of the Bjørnesund and Ravns Storø Supracrustal Belts, southern West Greenland: Settings for gold enrichment and corundum formation. Precambr. Res. 254, 36–58.
Keulen, N., Thomsen, T.B., Schumacher, J.C., Poulsen, M.D., Kalvig, P., Vennemann, T., Salimi, R., 2020. Formation, origin and geographic typing of corundum (ruby and pink sapphire) from the Fiskenæsset complex, Greenland. Lithos 366 (367), 105536.
Key, R.M., Ochieng, J.O., 1991. The growth of rubies in south-east Kenya. J. Gemmol. 22, 484–496.
Kokfelt, T.F., Thrane, K., Næraa, T., 2016a. Geochronology of Archaean Rocks. In: Kolb, J., Stensgaard, B.M., Kokfelt, T.F. (ed.), Geology and Mineral Potential of South-East Greenland. Danmarks Og Grønlands Geologiske Undersøgelse, Rapport 38, 28-36.
Kokfelt, T.F., Thrane, K. Johannesen, A.B., Arting; T.B., Weatherley, S., Keiding, J.K., Kolb, J., van Hinsberg, Næraa, T., 2016b. Paleoproterozoic intrusions. In: Kolb, J., Stensgaard, B.M., Kokfelt, T.F. (ed.), Geology and Mineral Potential of South-East Greenland 2016. Danmarks og Grønlands Geologiske Undersøgelse, Rapport 38, 56-71.
Kokfelt, T.F., Thrane, K., Næraa, T., Klausen, M.B., Tegner, C., 2016c. Geochronology of the Skjoldungen Alkaline province, South-East Greenland. Danmarks og Grønlands Geologiske Undersøgelse, Rapport 11, 124 pp.
Kolb, J., 2014. Structure of the Palaeoproterozoic Nagssugtoqidian Orogen, South-East Greenland: Model for the tectonic evolution. Precambr. Res. 255, 809–822.
Kolb, J., Thrane, K., Bagas, L., 2013. Field relationship of high-grade Neo- to Mesoarchaean rocks of South-East Greenland: tectonometamorphic and magmaticevolution. Gondw. Res. 23, 471–492.
Kolb, J., Stenagaard, B.M., Kokfelt, T.F., 2016. Geology and Mineral Potential of South-East Greenland. Danmarks Og Grønlands Geologiske Undersøgelse, Rapport 38, 156 pp.
Krebs, M.Y., Pearson, D.G., Fagan, A.J., Bussweiler, Y., Sarkar, C., 2019. The application of trace elements and Sr–Pb isotopes to dating and tracing ruby formation: The Aappaluttoq deposit, SW Greenland. Chemical Geology, Vol. 523, 30 September 2019, 42-58.
Kystol, J., Larsen, L.M., 1999. Analytical procedures in the Rock Geochemical Laboratory of the Geological Survey of Denmark and Greenland. GEUS Bulletin 184, 59–62.
La Touche, T., 1890. Sapphire mines of Kashmir. Rec. Geol. Surv. India 23, 59–69.
Lahtinen, R., Garde, A.A., Melezhik, V.A., 2008. Paleoproterozoic evolution of Fennoscandia and Greenland. Episodes 31, 20–28.
Langmuir, C. H., A. Bezos, S. Escrig, and S. W. Parman, 2006. Chemical systematics and hydrous melting of themantle in back-arc basins, in Back-Arc Spreading Systems. Geological, Biological, Chemical, and Physical Interactions Geophys. Monogr. Ser., Vol. 166, D. M. Christie (ed.) et al., AGU, Washington, D. C. 87-146.
Lawson, A.C., 1903. Plumasite, an oligoclase corundum rock, near Spanish Peak, California University of California. Pub. Geol. Sci. 3, 219–229.

Le Bas, M., Le Maitre, R., Streckeisen, A., Zanettin, B., 1986. A chemical classification of volcanic rocks based on the total alkali-silica diagram. J. Petrol. 27, 745–750.
Lebrun, E., Árting, T.B., Kolb, J., Fiorentini, M., Kokfelt, T.F., Johannesen, A.B., Maas, R., Thébaud, N., Martin, L.A.J., Murphy, R.C., 2018. Genesis of the Paleoproterozoic Ammassalik Intrusive Complex, south-east Greenland. Precambr. Res. 315, 19–44.
Li, X.-P., Rahn, M., Bucher, K., 2004. Serpentinites of the Zermatt-Saas ophiolite complex and their texture evolution. J. Metamorphic Geol. 22, 159–177.
Ludwig, K.R., 2012. User's manual for Isoplot version 3.75–4.15: a geochronological toolkit for Microsoft Excel. Berkeley Geochronological Center Special. Publication 5.
McDonough, W.F., Sun, S.-S., 1995. The composition of the Earth. Chem. Geol. 120 (1994), 223–253.
McLennan, S.M., Hemming, S., McDaniel, D.K., Hanson, G.N., 1993. Geochemical approaches to sedimentation, provenance and tectonics. In: Johansson, M.J., Basu, A. (ed.), Processes Controlling the Composition of Clastic Sediments. 284. Geological Society America, Special Paper, 21-40.
Meng, F., Shmelev, V.R., Kulikova, K.V., Ren, Y., 2018. A red-corundum-bearing vein in the Rai-Iz ultramafic rocks, Polar Urals, Russia: The product of fluid activity in a subduction zone. Lithos 320–321, 302–314.
Mercier, A., Debat, P., Saul, J.M., 1999. Exotic origin of the ruby deposits of the Mangari area in SE Kenya. Ore Geol. Rev. 1999 (14), 83–104.
Moreno, T., Gibbons, W., Prichard, H.M., Lunar, R., 2001. Platiniferous chromitite and the tectonic setting of ultramafic rocks in Cabo Ortegal, NW Spain. J. Geol. Soc. Lond. Vol. 2001, 158, 601–614.
Müller, S., Dziggel, A., Kolb, J., Sindern, S., 2018a. Mineral textural evolution and PT-path of relict eclogite-facies rocks in the Paleoproterozoic Nagssugtoqidian Orogen, South-East Greenland. Lithos 296–299, 212–232.
Müller, S., Dziggel, A., Sindern, S., Kokfelt, T.F., Gerdes, A., Kolb, J., 2018b. Age and temperature-time evolution of retrogressed eclogite-facies rocks in the Paleoproterozoic Nagssugtoqidian Orogen, South-East Greenland: Constrained from U-Pb dating of zircon, monazite, titanite and rutile. Precambr. Res. 314, 468–486.
Myers, J.S., 1984. The Nagssugtoqidian mobile belt of Greenland, Ammassalik region. In: Kröner, A., Greil-ing, R. (Eds.), Precambrian Tectonics Illustrated. Schweitzerbart, Stuttgardt, pp. 237–250.
Myers, J.S., 1987. The East Greenland Nagssugtoqidian mobile belt compared with the Lewisian complex. In: Park, R.G., Tarney, J. (eds.), Evolution of the Lewisian and Comparable Precambrian High Grade Terranes. Geological Society, London, Special Publication 27, 235-246.
Nicoli, G., Thomassot, E., Schannor, M., Vezinet, A., Jovovic, I., 2017. Constraining a Precambrian Wilson Cycle lifespan: An example from the ca. 1.8 Ga Nagssugtoqidian Orogen, Southeastern Greenland. Lithos 296–299, 1–16.
Nielsen, T.F.D., 1986. The Precambrian of South East Greenland – an introduction. Grønlands Geologiske Undersøgelse (GGU)15/2-1986, 40 pp.
Nilsson, M., Klausen, M.B., Petersson, A., 2019. Break-up related 2170–2120 Ma mafic dykes cross the North Atlantic craton: Final dismembering of a North Atlantic-Dharwar craton connection? Precambr. Res. 329, 70–87.
Nunes, P.D., Steiger, R.H., Bridgwater, D., 1974. A zircon age from gabbro-anorthosite inclusions in the gneisses of the Angmassalik area, South-East Greenland. Rapport Grønlands geologiske Undersøgelse. 66, 21–31.
Nutman, A.P., Friend, C.R.L., 1989. Reconnaissance PT studies of Proterozoic crustal evolution in the Ammassalik area, East Greenland. In: Kalsbeek, F. (ed.), Geology of the Ammassalik region, South-East Greenland. Grønlands Geologiske Undersøgelse, Rapport 146, 48-53.
Nutman, A.P., Kalsbeek, F., Friend, C.R.L., 2008. The Nagssugtoqidian orogen of South-East Greenland: evidence for Palaeoproterozoic collision and plate assembly. Am. J. Sci. 308, 529–572.
Palmer, K.F., 1971. A comparative study of two Precambrian Gneiss areas – The Suportoq region, East Greenland and South Harris, Outer Hebrides – and their bearing on Precambrian Crustal Evolution. PhD Thesis, July 1971, University of Birmingham, vol 1. 257 pp.
Paton, C., Woodhead, J.D., Hellstrom, J.C., Hergt, J.M., Greig, A., Maas, R., 2010. Improved laser ablation U-Pb zircon geochronology through robust downhole fractionation correction. Geochem. Geophys. Geosyst. 11, 1–36.
Paton, C., Hellstrom, J.C., Paul, P., Woodhead, J.D., Hergt, J.M., 2011. Iolite: Freeware for the visualisation and processing of mass spectrometric data. J. Anal. At. Spectrom 26, 2508–2518.
Pearce, J.A., 2008. Geochemical fingerprinting of oceanic basalts with applications to ophiolite classification and the search for Archean oceanic crust. Lithos. Vol. 100, Issues 1-4, January 2008, 14-48.
Pedersen, M., Weng, W.L., Keulen, N., Kokfelt, T.F., 2013. A new seamless digital 1:500 000 scale geological map of Greenland. Geol. Survey Denmark and Greenland Bulletin 28, 65–68.
Peters, S.T.M., Szilas, K., Sengupta, S., Kirkland, C.L., Garbe-Schönberg, D., Pack, A., 2020. >2.7Ga metamorphic peridotites from southeast Greenland record the oxygen isotope composition of Archean seawater. Earth Planet. Sci. Lett. 544, 116331.
Petrus, J.A., Kamber, B.S., 2012. VizualAge: A Novel Approach to Laser Ablation ICP-MS U-Pb Geochronology Data Reduction. Geostand. Geoanal. Res. 36, 247–270.
Poulsen, M.D., Paulick, H., Rosa, D., van Hinsberg, V.J., Petersen, J., Thomsen, L.L., 2015. Follow-up on Ujarassiorit mineral hunt finds andoutreach activities, South-East Greenland. Geol. Survey Denmark Greenland Bull. 33, 53–56.
Pratt, J.H., 1901. The occurrence and distribution of corundum in the United States. Geol. Surv. Bull. 180, 98. Senoble, J.B. An expedition to Tanzania's new ruby deposit in Winza. InColor 2008, 44–45.
Robb, L.J., Robb, V.M., 1986. Archean pegmatite deposits in the North-Eastern Transvaal. Mineral Deposits S. Afr. 1–2, 437–449.
Rollinson, H., Appel, P.W.U., Frei, R., 2002. A metamorphosed, early Archaean Chromitite from West Greenland: implications for the genesis of archaean anorthositic chromitites. J. Petrol. 43, 2143–2170.
Schreyer, W., 1988. A discussion of: "Corundum, Cr-muscovite rocks at O'Briens, Zimbabwe: the conjunction of hydrothermal desilicification and LIL-element enrichment – geochemical and isotopic evidence". Contrib. Mineral. Petrol. 100, 552–554.
Seifert, A.V., Hyrsl, J., 1999. Sapphire and garnet from Kalalani, Tanga Province. Tanzania. Gems Gemol. 35, 108–120.
Simonet, C., 2000. Géologie des gisements de saphir et de rubis— L'exemple de la John Saul Ruby Mine, Mangare, Kenya. Unpublished Ph.D. thesis, University of Nantes, France, 349 pp.
Simonet, C., Fritsch, E., Lasnier, B., 2008. A classification of gem corundum deposits aimed towards gem exploration. Ore Geol. Rev. 34, 127–133.
Slama, J., Kosler, J., Condon, D.J., Crowley, J.L., Gerdes, A., Hanchar, J.M., Horstwood, M.S.A., Morris, G.A., Nasdala, L., Norberg, N., Schaltegger, U., Schoene, N., Tubrett, M.N., Whitehouse, M.J., 2008. Plesovice zircon - a new natural reference material for U-Pb and Hf isotopic microanalysis. Chem. Geol. 249 (1–2), 1–35.
Smith, C.P., Fagan, A.J., Clark, B., 2016. Ruby and Pink Sapphire from Aappaluttoq, Greenland. J. Gemmol. 35(4), 2016, 294-306.
Sorokina, E.S., Rassomakhin, M.A., Nikandrov, S.N., Karampelas, S., Kononkova, N.N., Nikolaev, A.G., Anosova, M.O., Somsikova, A.V., Kostitsyn, Y.A., Kotlyarov, V.A., 2019. Origin of Blue Sapphire in Newly Discovered Spinel–Chlorite–Muscovite Rocks within Meta-Ultramafites of Ilmen Mountains, South Urals of Russia: Evidence from Mineralogy, Geochemistry, Rb-Sr and Sm-Nd Isotopic Data. Minerals 9, 36. https://doi.org/10.3390/min9010036.
Stensgaard, B.M, Kolb, J., Kokfelt, T.F, Klausen, M.B., 2016: Digital revised 1:500.000 geological map of South-East Greenland 62°00'N – 67°00'N and 33°00'W – 44°00'W Geological Survey of Denmark and Greenland (GEUS).
Stern, R.J., Tsujomori, T., Harlow, G., Groat, L.A., 2013. Plate tectonic gemstones. Geology, July 2013, Vol. 41, no. 7, 723-726. doi:10.1130/G34204.1.
St-Onge, M., van Gool, J.A.M., Garde, A.A., Scott, D., 2009. Correlation of Archaean and Palaeoproterozoic units between northeastern Canada and western Greenland: constraining the pre-collisional upper plate accretionary history of the Trans-Hudson orogen. Accretionary Orogens in Space and Time. Geological Society, London, Special Publications 318.
Tarney, J., Skinner, A.C., Sheraton, J.W., 1972. A geochemical comparison of Major Archaean Gneiss Units from Northwest Scotland and East Greenland. Proceedings of the 24th International Geological Congress, Section 1, 162-174.
Thomsen, T.B., Heijboer, T., Guarnieri, P., 2016. jAgeDisplay: software for evaluation of data distributions in U-Th-Pb geochronology. Geol. Survey Denmark Greenland Bull. 35, 103106.
Thrane, K., Kokfelt, T.F., Næraa, T., Árting, T.B., Lebrun, E., 2016. Geochronology Palaeoproterozoic rocks. In: Kolb, J., Stensgaard, B.M., Kokfelt, T.F. (ed.), Geology and Mineral Potential of South-East Greenland. Danmarks Og Grønlands Geologiske Undersøgelse, Rapport 38, 68-71.
Todt, W., Clif, R.A., Hanser, A., Hofmann, A.W., 1993. Re-calibration of NBS lead standards using 202Pb+205Pb double spike. Terra Abstr 5, 396.
Vakhrusheva, N.V., Ivanov, K.S., 2018. The nature and age of plagioclasites in the ultrabasic Rai-Iz massif (Polar Urals). Dokl. Earth Sci. 2018 (480), 587–590.
van Gool, J.A.M., Connelly, J.N., Marker, M., Mengel, F.C., 2002. The Nagssugtoqidian Orogen of West Greenland: tectonic evolution and regional correlations from a West Greenland perspective. Can. J. Earth Sci. 39, 665–686.
van Gool, J.A.M., 2006. Ruby Showings on Storø. Geological Survey of Greenland and Denmark (GEUS) Preliminary report with field notes and geologic map, 7 pp.
Vermeesch, P., Pease, V., 2021. A genetic classification of the tholeiitic and calc-alkaline magma series. Geochem. Perspect. Lett. Vol. 19 | https://doi.org/10.7185/geochemlet.2125.
Voudouris, P., Mavrogonatos, C., Graham, I., Giuliani, G., Melfos, V., Karampelas, S., Karantoni, V., Wang, K., Tarantola, A., Khin, Z., et al. 2019. Gem Corundum deposits of Greece: Geology, mineralogy and genesis. Minerals 2019, 9, 41 pp.
Wager, L.R., 1934. Geological investigations in East Greenland. Part 1. General geology from Angmagsalik to Kap Dalton. Medd. Grønland 105 (2), 46 pp.
Wager, L.R., Hamilton, E.I., 1964. Some radiometric rock ages and the problem of the Southward Continuation of the East Greenland Caledonian Orogeny. Nature 204 (December 12), 1079–1080.
Warr, L.N., 2021. IMA–CNMNC approved mineral symbols. Mineral. Mag. 2021 (85), 291–320. https://doi.org/10.1180/mgm.2021.43.
Wiedenbeck, M., Allé, P., Corfu, F., Griffin, W.L., Meier, M., Oberli, F., von Quadt, A., Roddick, J.C., Spiegel, W., 1995. Three natural zircon standards for U-Th-Pb, Lu-Hf, trace element and REE analyses. Geostand. Newslett. 19, 1–23.
Wiedenbeck, M., Hanchar, J.M., Peck, W.H., Sylvester, P., Valley, J., Whitehouse, M., Kronz, A., Morishita, Y., Nasdala, L., Fiebig, J., Franchi, I., Girard, J.-P., Greenwood, R.C., Hinton, R., Kita, N., Mason, P.R.D., Norman, M., Ogasawara, M., Piccoli, P.M., Rhede, D., Satoh, H., Schulz-Dobrick, B., Skår, Ø., Spicuzza, M.J., Terada, K., Tindle, A., Togashi, S., Vennemann, T., Xie, Q., Zheng, Y.-F., 2004. Further characterisation of the 91500 zircon crystal. Geostand. Geoanal. Res. 28, 9–39.
Wright, A.E., Tarney, J., Palmer, K.F., Moorlock, B.S.P., Skinner, A.C., 1973. The geology of the Angmagssalik area, East Greenland and possible relationsships with the Lewisian of Scotland. The Early Precambrian of Scotland and related rocks. Park, R. G. (ed.) and Tarney, J., University of Keele, 1973.
Wu, T., Polat, A., Frei, R., Fryer, B.J., Yang, K.-G., Kusky, T., 2016. Geochemistry, Nd, Pb and Sr isotope systematics, and U-Pb zircon ages of the Neoarchean Bad Vermilion Lake greenstone belt and spatially associated granitic rocks, western Superior

Province, Canada. Precambr. Res. 282, 21–51. https://doi.org/10.1016/j.precamres.2016.06.021.
Yakymchuk, C., Szilas, K., 2018. Corundum formation by metasomatic reactions in Archean metapelite, SW Greenland: Exploration vectors for ruby deposits within high-grade greenstone belts. Geosci. Front. 9, 727–749.
Yakymchuk, C., Hinsberg, V.V., Kirkland, C.L., Szilas, K., Kinney, C., Kendrick, J., Hollis, J.A., 2021. Corundum (ruby) growth during the final assembly of the Archean North Atlantic Craton, southern West Greenland. Ore Geol. Rev. 138, 18 pp, 104417.